MOLECULAR AND CELLULAR BIOLOGY, Apr. 2009, p. 1834–1854 Vol. 29, No. 7
0270-7306/09/$08.00+0 doi:10.1128/MCB.01337-08

APE1/Ref-1 Interacts with NPM1 within Nucleoli and Plays a Role in the rRNA Quality Control Process▽†

Carlo Vascotto,[1]‡ Damiano Fantini,[1]‡ Milena Romanello,[1] Laura Cesaratto,[1] Marta Deganuto,[1] Antonio Leonardi,[3] J. Pablo Radicella,[4] Mark R. Kelley,[5,6,7] Chiara D'Ambrosio,[2] Andrea Scaloni,[2] Franco Quadrifoglio,[1] and Gianluca Tell[1]*

Department of Biomedical Sciences and Technologies, University of Udine, 33100 Udine, Italy[1]; Proteomics and Mass Spectrometry Laboratory, ISPAAM, National Research Council, 80147 Naples, Italy[2]; Dipartimento di Biologia e Patologia Cellulare e Molecolare, Federico II University of Naples, 80131 Naples, Italy[3]; CEA, Institut de Radiobiologie Cellulaire et Moléculaire, UMR217 CNRS, 92265 Fontenay-aux-Roses, France[4]; and Department of Pediatrics, Herman B Wells Center for Pediatric Research,[5] and Departments of Biochemistry and Molecular Biology[6] and Pharmacology and Toxicology,[7] Indiana University School of Medicine, 1044 W. Walnut, Indianapolis, Indiana

Received 22 August 2008/Returned for modification 29 September 2008/Accepted 20 January 2009

APE1/Ref-1 (hereafter, APE1), a DNA repair enzyme and a transcriptional coactivator, is a vital protein in mammals. Its role in controlling cell growth and the molecular mechanisms that fine-tune its different cellular functions are still not known. By an unbiased proteomic approach, we have identified and characterized several novel APE1 partners which, unexpectedly, include a number of proteins involved in ribosome biogenesis and RNA processing. In particular, a novel interaction between nucleophosmin (NPM1) and APE1 was characterized. We observed that the 33 N-terminal residues of APE1 are required for stable interaction with the NPM1 oligomerization domain. As a consequence of the interaction with NPM1 and RNA, APE1 is localized within the nucleolus and this localization depends on cell cycle and active rRNA transcription. NPM1 stimulates APE1 endonuclease activity on abasic double-stranded DNA (dsDNA) but decreases APE1 endonuclease activity on abasic single-stranded RNA (ssRNA) by masking the N-terminal region of APE1 required for stable RNA binding. In APE1-knocked-down cells, pre-rRNA synthesis and rRNA processing were not affected but inability to remove 8-hydroxyguanine-containing rRNA upon oxidative stress, impaired translation, lower intracellular protein content, and decreased cell growth rate were found. Our data demonstrate that APE1 affects cell growth by directly acting on RNA quality control mechanisms, thus affecting gene expression through posttranscriptional mechanisms.

APE1/Ref-1 (also called HAP1 or APEX, and here referred to as APE1), the mammalian ortholog of *Escherichia coli* Xth (exonuclease III), is a vital protein (20) that acts as a master regulator of cellular response to oxidative stress conditions and contributes to the maintenance of genome stability (55, 56). APE1 is involved in both the base excision repair (BER) pathways of DNA lesions, acting as the major apurinic/apyrimidinic (AP) endonuclease, and in transcriptional regulation of gene expression as a redox coactivator of different transcription factors, such as early growth response protein 1 (Egr-1), NF-κB, and p53 (55, 56). These two biological activities are located in two functionally distinct protein domains. In fact, the N-terminal region, containing the nuclear localization signal (NLS) sequence, is principally devoted to redox activity through Cys65, while the C-terminal one exerts enzymatic activity on the abasic sites of DNA (56, 63). The protein C terminus is highly conserved during phylogenesis, while the N terminus is not. Except in mammals, which always show a high sequence conservation (more than 90%), and *Danio*, *Drosophila*, *Xenopus*, and *Dictyostelium* (presenting a sequence identity of less than 40%), the N-terminal region is mostly absent in other organisms. A third APE1 function, which is regulated by Lys6/Lys7 acetylation (7), is indirect binding to the negative calcium response elements (nCaRE) of some promoters (i.e., PTH and APE1 promoters), thus acting as a transcriptional repressor (12, 30).

In different mammalian cell types, the APE1 subcellular distribution is mainly nuclear and is critical for controlling cellular proliferative rate (20, 25, 28). However, cytoplasmic, mitochondrial, and endoplasmic reticulum localization has also been reported (11, 22, 33, 50, 54). Interestingly, cytoplasmic expression of APE1 has been correlated with aggressiveness of different tumors (55, 56), although its role in tumorigenic processes is completely unknown. To date, no subnuclear distribution of APE1 has been reported. APE1 is an abundant protein (about 10^4 to 10^5 copies/cell) within eukaryotic cells and has a relatively long half-life (about 8 h). Thus, fine-tuning of the multiple APE1 functions may reside on its posttranslational modifications and on the modulation of its interactome under different conditions. While some posttranslational modifications have a functional role (i.e., Lys6/Lys7 acetylation) (7, 17), little information is available on APE1 protein interacting

* Corresponding author. Mailing address: Department of Biomedical Sciences and Technologies, University of Udine, P.le Kolbe 4, 33100 Udine, Italy. Phone: 39 0432 494311. Fax: 39 0432 494301. E-mail: gianluca.tell@uniud.it.

† Supplemental material for this article may be found at http://mcb.asm.org/.

‡ C.V. and D.F. contributed equally to the present work.

▽ Published ahead of print on 2 February 2009.

partners, except for those that are involved in BER function (38).

Interestingly, proteolysis at residue Lys31 has recently been related to an enhanced immune cell death mediated by granzymes A and K (16, 23). This proteolytic event reduces APE1 accumulation within nuclei (16, 29) and its interaction with XRCC1 (60) and alters APE1 functions (16, 23). Recently, proteolysis occurring at Asn33 (giving rise to a protein form called NΔ33APE1) has also been described (11), suggesting that removal of the NLS may constitute a general mechanism for redirecting APE1 toward noncanonical subcellular compartments, such as mitochondria (11, 33, 54). Unfortunately, neither has the specific protease responsible for this cleavage been identified in nonimmune cells, nor has the mitochondrial localization signal been mapped yet. Mitochondrial localization of APE1 could be associated with a potential role in mtDNA repair of oxidized bases (11, 33, 54). However, since it is not clear whether NΔ33APE1 maintains its DNA repair activity in vivo (16) or acquires an aspecific endonuclease activity for double-stranded DNA (dsDNA) (66), at present it is not possible to drive any definitive conclusion. Moreover, as the truncated NΔ33APE1 form is associated with an apoptotic phenotype (23), it cannot be excluded that its generation may causatively be involved in the cytotoxic effect, driving proapoptotic triggering directly within mitochondria.

The first 42 amino acids of APE1 are highly unordered in the protein crystallographic structure (3, 35), while the remainder of the protein has a globular fold (21). It is therefore presumable that the protein's N terminus is used for interacting with other partners, thus modulating the different APE1 functions. Interestingly, a similar bipartite arrangement for Rrp1, the *Drosophila* homologue of mammalian APE1, has been described, pointing out a functional role of the unstructured N-terminal domain in modulating protein-protein interactions (42, 52).

By using an unbiased proteomic approach, in this work we have identified and characterized a novel APE1 complex. We found that APE1 N terminus is essential for binding to a number of proteins involved in ribosome biogenesis and RNA processing. Among the interacting partners, we focused on the nucleophosmin (NPM1)-APE1 interaction. NPM1 is an abundant protein which specifically resides within the granular region of the nucleolus and has been implicated in a variety of cellular processes, including centrosome duplication, maintenance of the genome's integrity, and ribosome biogenesis (19). NPM1 has a chaperone activity regulated by phosphorylation (51) and an endoribonuclease activity at a specific site of the spacer region between the 5.8S and the 28S rRNAs (43). Here, we demonstrate that the NPM1-APE1 interaction is required for APE1 subnuclear localization and for modulating the cleansing process of rRNA. Our data demonstrate that APE1 affects cell growth by directly acting on RNA quality control mechanisms, thus possibly affecting gene expression through posttranscriptional mechanisms.

MATERIALS AND METHODS

Inducible siRNA of APE1 and generation of APE1-knock-in cell lines. The following oligonucleotides were used for the short hairpin RNA (shRNA) of APE1: sense, 5′-GATCCCCCCTGCCACACTCAAGATCTGCTTCAAGAGAGCAGATCTTGAGTGTGGCAGGTTTTTGGAAA-3′; and antisense, 5′-AGCTTTTCCAAAAACCTGCCACACTCAAGATCTGCTCTCTTGAAGCAGATCTTGAGTGTGGCAGGGGG-3′. These sequences were drawn following the empirical rules of Mittal (34) and were designed to recognize and bind to a 21-base sequence (underlined) placed 175 nucleotides after the AUG initiation codon of the APE1 gene. As a control, we used the following scrambled oligonucleotide sequences: sense, 5′-GATCCCCAGTCTAACTCGCCACCCCGTATTCAAGAGATACGGGGTGGCGAGTTAGACTTTTTTGGAAA-3′; antisense, 5′-AGCTTTTCCAAAAAAGTCTAACTCGCCACCCCGTATCTCTTGAATACGGGGTGGCGAGTTAGACTGGG-3′. These sequences were checked with BLAST (http://www.ncbi.nlm.nih.gov/blast/) for their inability to pair with any human cDNA sequence. The sequences were cloned into BglII and HindIII restriction sites of pTER vector (57), which presents a tetracycline (doxycycline)-responsive promoter to form the so-called pTER/APE1 vector and pTER/Scr, respectively. In the first step, HeLa cells were transfected with pcDNA6/TR to generate stable Tet repressor-expressing cell clones that were selected for the acquired resistance by incubation with 5 μg/ml blasticidin (Invitrogen, Milan, Italy) for 14 days. Individual clones were isolated by using cell cloning cylinders (Sigma, Milan, Italy), transferred, and grown stepwise into 24-well, 12-well, and 6-well plates for expansion to 10^7 cells. Clone TR5 expressed the Tet repressor at the highest levels and was therefore selected for transfection with pTER/APE1 vector previously linearized with Bst1107I (Fermentas, St. Leon Rot, United Kingdom) and subjected to selection with Zeocin (200 μg/ml) (Invitrogen) for 14 to 21 days. Thirty single clones were isolated by using cell cloning cylinders, transferred, and grown stepwise for expansion to 10^7 cells. As a control, we used cell clones transfected with the empty pTER vector or with pTER/Scr vector. For inducible siRNA experiments, doxycycline (Sigma) was added to the cell culture medium at the final concentration of 1 μg/ml and cells were grown for 10 days. Total cellular extracts were analyzed for APE1 expression by immunoblotting. The HeLa control cell clone was identified as siScr, while the APE1-knocked-down cell clone was identified as siAPE1 (58).

For generation of APE1 knock-in cell lines, an APE1 expression vector was generated by cloning an EcoRI-BamHI fragment from pFLAG-CMV-5.1/APE1 (Sigma) into p3XFLAG-CMV-14 vector (Sigma). To avoid the degradation of the ectopic APE1 mRNA by the specific siRNA sequence described above, two nucleotides of the APE1-cDNA coding sequence were mutated with site-directed mutagenesis kits (Stratagene), leaving the APE1 amino acid sequence unaffected: siRNA, 5′-CCTGCCACACTCAAGATCTGC-3′; and APE1, 5′-CCTGCAACGCTCAAGATCTGC-3′. The NΔ33APE1 deletion mutant was generated by PCR and subcloning from the full-length cDNA sequence. All of the mutants were confirmed by DNA sequencing. Then, the APE1 siRNA clone was transfected with p3XFLAG-CMV/APE1, the wild-type (WT) APE1, and a deletion mutant (NΔ33APE1), previously digested with ScaI (Fermentas); 48 h after transfection, the cells were subjected to selection with Geneticin (Invitrogen) for 14 days and selected for the acquired resistance. Individual clones were isolated by using cell cloning cylinders, transferred, and grown for expansion to 10^7 cells in the presence of selective antibiotics. As control, the siRNA control clone was transfected with the p3XFLAG-CMV-14 empty vector. After 10 days of doxycycline treatment at the final concentration of 1 μg/ml, total or nuclear and cytoplasmic cellular extracts were analyzed for APE1 expression by immunoblotting, thus revealing the silencing of the endogenus APE1 and the expression of the ectopic flagged WT and mutant forms of the protein. All biologic data were reproduced in at least two different cell clones for each model.

Cell culture and transient transfection experiments. HeLa cells were grown in Dulbecco's modified Eagle's medium (Invitrogen) supplemented with 10% fetal bovine serum (Euroclone, Milan, Italy), 100 U/ml penicillin, and 10 μg/ml streptomycin sulfate. One day before transfection, cells were seeded in 10-cm plates at a density of 1.8×10^6 cells/plate. Cells were then transiently transfected with 12 μg of either pFLAG5.1 (empty vector) or pFLAG5.1-APE1 plasmid per dish, using Lipofectamine 2000 reagent (Invitrogen) according to the manufacturer's instructions. Cells were harvested 48 h after transfection.

Preparation of cell extracts and anti-Flag coimmunoprecipitation. For preparation of total cell lysates and coimmunoprecipitation, cells were harvested by trypsinization and centrifuged at $250 \times g$ for 5 min at 4°C. Supernatant was removed, and the pellet was washed once with ice-cold phosphate-buffered saline (PBS) and then centrifuged again as described before. Cell pellet was resuspended in lysis buffer containing 50 mM Tris HCl (pH 7.4), 150 mM NaCl, 1 mM EDTA, and 1% [wt/vol] Triton X-100 supplemented with 1× protease inhibitor cocktail (Sigma), 0.5 mM phenylmethylsulfonyl fluoride (PMSF), 1 mM NaF, and 1 mM Na_3VO_4, at a cell density of 10^7 cells/ml and rotated for 30 min at 4°C. After centrifugation at $12{,}000 \times g$ for 10 min at 4°C, the supernatant was collected as total cell lysate. The protein concentration was determined using Bio-Rad protein assay reagent (Bio-Rad, Hercules, CA). Samples were then

coimmunoprecipitated for 3 h using anti-Flag M2 affinity gel (Sigma) following the manufacturer's instructions. Proteins were eluted by incubation with 0.15 mg/ml 3× Flag peptide in Tris-buffered saline (TBS) and subjected to Western blot analysis.

Nuclear protein extracts were prepared as described earlier (67). Briefly, cells were washed and scraped into cold PBS and then centrifuged at 2,000 × *g* for 10 min at 4°C. Supernatant was removed, and the pellet was resuspended in buffer A (10 mM Tris-HCl [pH 7.5], 1.5 mM $MgCl_2$, and 10 mM KCl supplemented with 1× protease inhibitor cocktail, 0.5 mM PMSF, 1 mM NaF and 1 mM Na_3VO_4) at a cell density of 3×10^7 cells/ml and incubated on ice for 10 min. The nuclei were collected by centrifugation at 2,000 × *g* for 10 min at 4°C and then resuspended in buffer B (20 mM Tris-HCl [pH 7.5], 0.42 M KCl, 1.5 mM $MgCl_2$, 20% [vol/vol] glycerol supplemented with 1× protease inhibitor cocktail, 0.5 mM PMSF, 1 mM NaF, and 1 mM Na_3VO_4) and rotated for 30 min at 4°C. The suspension was centrifuged at 15,000 × *g* for 30 min at 4°C and dialyzed against three changes of buffer C (25 mM Tris-HCl [pH 7.5], 0.2 mM EDTA, 0.1 M KCl, 20% [vol/vol] glycerol freshly supplemented with 1× protease inhibitor cocktail, 0.5 mM PMSF, 1 mM NaF, and 1 mM Na_3VO_4) for 4 h, at 4°C. The dialyzed sample was collected as nuclear protein extract and used for coimmunoprecipitation experiments.

2-DE differential proteomic analysis, evaluation of differentially represented spots, and mass spectrometry analysis. Ten micrograms of immunoprecipitated material from different samples was loaded onto 13-cm, pH 3 to 10 L IPG strips (GE Healthcare, Milan, Italy). Isoelectric focusing was conducted using an IPGPhor II system (GE Healthcare) according to the manufacturer's instructions. Focused strips were equilibrated with a mixture of 6 M urea, 26 mM dithiothreitol (DTT), 4% (wt/vol) sodium dodecyl sulfate (SDS), 30% (vol/vol) glycerol in 0.1 M Tris-HCl (pH 6.8) for 15 min, followed by 6 M urea, 0.38 M iodoacetamide, 4% (wt/vol) SDS, 30% (vol/vol) glycerol, and a dash of bromophenol blue in 0.1 M Tris-HCl (pH 6.8) for 10 min. The equilibrated strips were applied directly to 10% (wt/vol) SDS–polyacrylamide gels and separated at 130 V. Gels were fixed and stained with ammoniacal silver (47). Gels were scanned with an Image Scanner II apparatus and analyzed by the ImageMaster 2D Platinum software (GE Healthcare), which allowed estimation of relative differences in spot intensities for each represented protein.

Each sample was analyzed in triplicate, and then a comparative analysis was carried out as previously reported (59). Differential spots from two-dimensional electrophoresis (2-DE) were excised from the gel, triturated, and washed with water. Proteins were in-gel reduced, S alkylated, and digested with trypsin as previously reported (59). Digest aliquots were removed and subjected to a desalting/concentration step on μZipTip C_{18} column (Millipore Corp., Bedford, MA) using acetonitrile as the eluent before matrix-assisted laser desorption ionization–time of flight mass spectrometry analysis. Peptide mixtures were loaded on the matrix-assisted laser desorption ionization target, using the dried-droplet technique and α-cyano-4-hydroxycinnamic acid as the matrix, and analyzed by using a Voyager-DE PRO mass spectrometer (Applied Biosystems, Framingham, MA). Spectra were elaborated using the DataExplorer 5.1 software (Applied Biosystems) and manually inspected to get the peak lists. Internal mass calibration was performed with peptides deriving from enzyme autoproteolysis. PROWL and Matrix Science software packages were used to identify spots unambiguously from all updated taxa from the NCBI nonredundant sequence database (NCBInr 20080610, containing 6,573,034 protein sequences) by using a mass tolerance value of 50 to 70 ppm, trypsin as the enzyme specificity, a missed-cleavage maximum value of 2, and cysteine carbamidomethylation and methionine oxidation as the fixed and variable modifications, respectively. Candidates with ProFound's estimated Z scores of >1.8 and Mascot's scores of >81 were further evaluated by the comparison with their calculated mass and pI using the experimental values obtained from 2-DE.

Isolation of nucleoli. Nucleoli were isolated from HeLa cells by a variant of a method described earlier (37) and recently adapted for this particular cell line by Lamond and coworkers (http://lamondlab.com/f7nucleolarprotocol.htm). HeLa cells were seeded onto 10- by 14-cm petri dishes and cultured at 37°C in a 5% CO_2 atmosphere until 90% of confluence, corresponding to 10^7 cells/dish. An hour before nucleolar isolation, the medium was replaced with a fresh, prewarmed one. Cells were washed three times with PBS, harvested with trypsin-EDTA solution (2 ml/dish), and collected. The pellet was washed three times with cold PBS at 218 × *g* at 4°C, and after the final wash, the pellet was resuspended in 5 ml of buffer A (10 mM HEPES [pH 7.9], 10 mM KCl, 1.5 mM $MgCl_2$, 0.5 mM DTT) and incubated on ice for an additional 5 min. Then, the cell suspension was transferred to a precooled 7-ml Dounce tissue homogenizer, homogenized 10 times while keeping the cells on ice, and centrifuged at 218 × *g* for 5 min at 4°C. The pellet obtained contains entire, but not highly pure, nuclei. The pellet was resuspended with 3 ml of S1 solution (0.25 M sucrose, 10 mM $MgCl_2$), layered over 3 ml of S2 solution (0.35 M sucrose, 0.5 mM $MgCl_2$), and centrifuged at 1,430 × *g* for 5 min at 4°C. With this step, a cleaner nuclear pellet was obtained, which was resuspended in 3 ml of S2 solution and sonicated on ice for six 10-s bursts to disrupt the nuclear membrane. The sonicated sample was overlaid to 3 ml of S3 solution (0.885 M sucrose, 0.5 mM $MgCl_2$) and centrifuged at 3,000 × *g* for 10 min at 4°C. The pellet was resuspended with 0.5 ml of S2 solution and centrifuged at 1,430 × *g* for 5 min at 4°C. The resulting pellet contained highly purified nucleoli, which were resuspended in 0.5 ml of S2 solution and stored at −80°C or lysed with radioimmunoprecipitation assay (RIPA) buffer (50 mM Tris HCl [pH 8.0], 150 mM NaCl, 1% [wt/vol] NP-40, 0.5% [wt/vol] deoxycholate, 0.1% [wt/vol] SDS, protease inhibitor cocktail) to obtain highly purified nucleolar protein extracts. The products of each step of the protocol were checked by using a phase-contrast microscope.

Plasmids and expression of recombinant proteins. The construct pGex2T-APE1, coding for the glutathione *S*-transferase (GST)-APE1 full-length protein, was kindly provided by Sankar Mitra (University of Texas Medical Branch, Galveston, TX). The construct pGex2T-NΔ33APE1 deletion mutant, coding for the truncated APE1 lacking the first 33 N-terminal residues, was generated by subcloning from the previous one through PCR and confirmed by direct sequencing. The plasmids coding for GST-NPM1 full-length and GST-NPM1 deletion mutant proteins were kindly provided by P. G. Pelicci (European Institute of Oncology, Milan, Italy). For expression of His_6-tagged NPM1, cDNA coding for full-length NPM1 was cloned in the pET-15b-expressing plasmid (Invitrogen). All proteins were expressed in *E. coli* BL21(DE3), induced with 1 mM isopropyl-β-D-thiogalactopyranoside (IPTG), and then purified using the GSTrap HP column (GE Healthcare) in the case of GST-tagged proteins or the HisTrap HP column (GE Healthcare) in the case of His_6-NPM1. An AKTA Prime (GE Healthcare) fast protein liquid chromatography system was used for all purification steps. In some cases, purification to the homogeneity was obtained by a further gel filtration step. The quality of purification was checked by silver-stained SDS-polyacrylamide gel electrophoresis (PAGE) analysis. Extensive dialysis against PBS was performed to remove any trace of imidazole from the HisTrap-purified proteins.

Accurate quantification of all recombinant proteins was performed by colorimetric Bradford assays (Bio-Rad) and confirmed by SDS-PAGE and by Western blotting analysis using anti-GST peroxidase-conjugated antibody (Sigma). GST-APE1 and GST-NΔ33APE1 proteins were further hydrolyzed with thrombin (0.5 thrombin units per mg of recombinant GST-fused protein) to remove the GST tag. The protease was then removed from the sample using a benzamidine HiTrap FF column (GE Healthcare); and then APE1 was purified on a GSTrap HP column (GE Healthcare). This recombinant cleaved form of APE1 was identified as rAPE1 to differentiate it from the Flag-tagged and GST-tagged APE1 proteins.

GST pull-down assay. For the GST pull-down experiments, 0.1 nmol of either full-length GST-NPM1 or each GST-NPM1 deletion mutant protein was added, together with 0.1 nmol of APE1 protein, to 10 μl of glutathione-Sepharose 4B beads (GE Healthcare). Binding was performed in PBS supplemented with 5 mM DTT and 1× protease inhibitor cocktail for 2 h under rotation at 4°C. The beads were washed three times with washing buffer (PBS supplemented with 0.8% [wt/vol] Triton X-100, 5 mM DTT, 1× protease inhibitor cocktail). Beads were boiled in 1× Laemmli sample buffer containing 100 mM DTT for 5 min, and the supernatant was loaded onto 10% (wt/vol) SDS-PAGE gels followed by Western blotting. The presence of APE1 protein was detected using anti-APE1 monoclonal antibody, while the presence of NPM1 protein was revealed using anti-GST peroxidase-conjugated antibody (Sigma).

Cell cycle synchronization and flow cytometry. HeLa cells were synchronized at the G_1/S boundary by two cycles of thymidine blockage. Briefly, cells were seeded at 3×10^4 to 4×10^4 cells/cm^2 in six-well trays. After 24 h, cells were treated with 2 mM thymidine (Sigma) in complete medium for 19 h and then released in complete medium for 9 h and subjected to a second block with 2 mM thymidine for 16 h. After the double block, cells were released in complete medium and harvested at different time points. Cells were trypsinized, washed in PBS, fixed in cold 70% (vol/vol) ethanol, and stained for fluorescence-activated cell sorter (FACS) analysis in PBS containing 50 μg/ml propidium iodide, 0.1% (wt/vol) Triton X-100, and 10 μg/ml RNase A for 20 min on ice. Cells were then analyzed by FACS analysis using an Ar laser (excitation, 488 nm) on a Becton-Dickinson (Franklin Lakes, NJ) FACScan equipped with ModFitLT V3.0 software program.

Apoptosis measurements. Apoptosis was assessed by staining of phosphatidylserines exposed on cell membranes with fluorescein isothiocyanate-labeled annexin V, according to the manufacturer's instructions (Roche Diagnostic Italia, Monza, Italy). Samples were analyzed by flow cytometry using a FACScan. In addition, caspase 3/7 activation was measured by an immunofluorescent assay

(Apo-ONE homogeneous caspase assay; Promega Corp., Madison, WI) according to the manufacturer's instructions.

Immunofluorescence confocal analysis. For experiments on APE1-Flag/NCL or APE1/NPM1 colocalization, a sequential protocol of double immunofluorescence was used, based on labeled goat anti-mouse isotype-specific secondary antibodies. The nucleoli were detected with an antinucleolin (anti-NCL) (immunoglobulin G2b [IgG2b]) or an anti-NPM1 (IgG1) antibody (NCL, clone ZN004; NPM1, clone FC-61991 [Zymed Laboratories, Invitrogen]). Cells fixed in 4% (wt/vol) paraformaldehyde for 20 min at room temperature were permeabilized for 5 min with PBS–0.25% (wt/vol) Triton X-100 and incubated for 30 min with 5% normal goat serum in PBS–0.1% (wt/vol) Triton X-100 (blocking solution) to block unspecific binding of the antibodies. Cells were then incubated with the mouse monoclonal anti-FLAG (IgG1) (Sigma) or APE1 (IgG2b) antibody (39), diluted 1:1000 or 1:30, respectively, in blocking solution, for 2.5 h. After washing, cells were incubated for 90 min with secondary antibody: Alexa Fluor 488-conjugated goat anti-mouse IgG1 or Alexa Fluor 546-conjugated goat anti-mouse IgG2b (1:200) (Molecular Probes, Invitrogen). After washing, a second blocking step for 30 min in the dark was performed, and then the cells were incubated overnight at 4°C with the second primary antibody—5 μg/ml mouse anti-NCL (IgG2b) or mouse anti-NPM1 (IgG1) in blocking solution. After washing, cells were incubated for 90 min with secondary antibody Alexa Fluor 546-conjugated goat anti-mouse IgG2b or Alexa Fluor 488-conjugated goat anti-mouse IgG1 (1:200; Molecular Probes). The preparations were then washed with PBS three times for 5 min each in the dark. Nuclei were then stained by 5 min of incubation in 300 nM solution of 4′,6-diamidino-2-phenylindole dihydrochloride (DAPI) (Sigma) in PBS. The preparations were then washed three times in PBS for 5 min. The microscope slides were then mounted onto slides in Mowiol 4-88 supplemented with DABCO (1:5) as an anti-fade reagent. Coverslips were visualized through a Leica TCS SP laser-scanning confocal microscope (Leica Microsystems, Wetzlar, Germany) equipped with a 488-nm argon laser, a 543-nm HeNe laser, and a 63× oil fluorescence objective.

Actinomycin D (ActD; Sigma) solution was prepared in dimethyl sulfoxide (DMSO). Cells were treated with 1 μg/ml of ActD or vehicle for 40, 80, and 180 min, as previously described (1).

RNase A treatments were performed with certified DNase-free chromatographically purified RNase A (Sigma catalog no. R6513). This protocol was a modification of the previously published protocol (32). Fixed cells were permeabilized with 0.25% (wt/vol) Triton X-100 for 6 min at room temperature, washed with PBS, incubated with 0.1 mg/ml RNase A (Sigma catalog no. R6513) in PBS for 30 min at 37°C, washed three times with PBS–0.1% (wt/vol) Triton X-100 for 5 min, and then processed for immunofluorescence. All experiments were also performed with RNase A (Sigma catalog no. R5125) after inactivation of residual contaminants by boiling at 100°C for 15 min, always obtaining the same results.

Western blot analysis and antibodies. The indicated amounts of cell extracts were electrophoresed onto a 12% SDS-PAGE. Proteins were then transferred to nitrocellulose membranes (Schleicher & Schuell, Keene, NH). Membranes were saturated by incubation at 4°C overnight with 5% (wt/vol) nonfat dry milk in PBS–0.1% (wt/vol) Tween 20 and then incubated with the polyclonal anti-APE1 antibody (39) for 3 h. In the case of anti-NPM1 and anti-NCL, the specific antibodies from Zymed (Invitrogen) were used. After three washes with PBS–0.1% (wt/vol) Tween 20, membranes were incubated with an antirabbit Ig coupled to peroxidase (Sigma). After 60 min of incubation at room temperature, the membranes were washed three times with PBS–0.1% Tween 20 and the blots were developed using the ECL enhanced chemiluminescence procedure (GE Healthcare). Normalization was performed with the polyclonal antiactin or anti-β-tubulin antibodies (Sigma). Blots were quantified by using a Gel Doc 2000 video densitometer (Bio-Rad).

Coimmunoprecipitation and rRNA qRT-PCR. HeLa cells were transiently transfected with APE1-Flag-, ΔN33-Flag-, or NPM1-Flag-expressing plasmids, as described above. Forty-eight hours after transfection, the cells were harvested by trypsinization and centrifuged at 250 × *g* for 5 min, at 4°C. Supernatant was removed, and the pellet was washed once with ice-cold PBS and centrifuged again as described before. The cell pellet was resuspended in lysis buffer (50 mM Tris HCl [pH 7.4], 150 mM NaCl, 1 mM EDTA, 1% Triton X-100 supplemented with 1× protease inhibitor cocktail, 0.5 mM PMSF, 1 mM NaF, 1 mM Na_3VO_4, and 0.5 U/ml RNaseOUT [Invitrogen]) at a cell density of 10^7 cells per ml and then rotated for 30 min at 4°C. After centrifugation at 12,000 × *g* for 10 min, at 4°C, the supernatant was collected as total cell lysate. A fraction of each input lysate was analyzed to quantify the total starting RNA. Total RNA was extracted and purified using Trizol reagent (Invitrogen) according to the manufacturer's instructions. The RNA concentration was obtained spectrophotometrically, and RNA integrity was checked on agarose-formaldehyde gels. Different amounts of lysates, corresponding to the same quantity of total starting RNA, were subjected to coimmunoprecipitation for 1 h using anti-Flag M2 affinity gel (Sigma), following the manufacturer's instructions. Elution was performed by incubation with 0.15 mg/ml 3× Flag peptide in TBS supplemented with 0.5 U/ml RNaseOUT. Immunoprecipitates were then subjected to Western blot analysis or RNA extraction using Trizol reagent, according to the manufacturer's instructions. Immunoprecipitated RNA was furthermore analyzed by quantitative real-time reverse transcription-PCR (qRT-PCR) to determine for the presence of the specific rRNA molecules coeluted with APE1 and NPM1 proteins.

Levels of 47S, 28S, and 18S rRNA transcripts were determined by methods similar to those previously described (2). Total RNA was reverse transcribed using the iScript cDNA synthesis kit (Bio-Rad) according to the manufacturer's instructions. qRT-PCR was performed with iQ5 multicolor real-time PCR detection system (Bio-Rad), according to the manufacturer's protocol. The following primers were used: 47S_for (5′-CGCCGCGCTCTACCTTACCTA-3′) and 47S_rev (5′-TAGGAGAGGAGCGAGCGACCA-3), which amplified a region of 174 bp; 18S_for (5′-CTGCCCTATCAACTTTCGATGGTAG-3′) and 18S_rev (5′-CCGTTTCTCAGGCTCCCTCTC-3′), which amplified a region of 100 bp; and 28S_for (5′-TGTCGGCTCTTCCTATCATTGT-3′) and 28S_rev (5′-ACCCAGCTCACGTTCCCTATTA-3′), which amplified a region of 81 bp.

cDNA was amplified in 96-well plates using primers for 18S, 28S, and 47S rRNA in separate wells using the 2X iQ SYBR green supermix (Bio-Rad) (100 mM KCl, 40 mM Tris-HCl [pH 8.4], 0.4 mM each deoxynucleoside triphosphate [dNTP], 50 U/ml iTaq DNA polymerase, 6 mM $MgCl_2$, SYBR green I, 20 nM fluorescein, and stabilizers) and 300 nM of the specific sense and antisense primers in a final volume of 15 μl for each well. Each sample analysis was performed in triplicate. As negative control, a sample without template was used; as control for genomic DNA contamination, a sample with non-retro-transcribed mRNA was included instead of template cDNA. The cycling parameters were denaturation at 95°C for 10 s and annealing/extension at 60°C for 30 s (repeated 40 times). In order to verify the specificity of the amplification, a melting-curve analysis was performed, immediately after the amplification protocol.

A standard curve was generated by using a calibrating cDNA. This cDNA was obtained from a retrotranscription of 1 μg of total RNA from input samples, which was serially diluted and analyzed for 47S, 18S, and 28S rRNA. We assumed that rRNA represented 90% of the total RNA in a molar ratio between 28S and 18S rRNA of 2:1. By using the equation describing the plots of the $\log_{10}$ of the starting amount of 5 dilutions of the calibrator cDNA versus the corresponding threshold cycle, the iQ5 optical system software calculated the amount of the template for each sample.

Evaluation of oxidized RNA through immunofluorescence and quantification of 8-OHG rRNA by immunoprecipitation, qRT-PCR, and Northwestern analysis. For immunofluorescence analysis of 8-hydroxyguanine (8-OHG)-modified RNA, HeLa cells were plated onto glass coverslips. The day after plating, the cells were maintained for 1 h in serum-free medium and then treated for 1 h with 50 μM H_2O_2 or vehicle. The cultures were fixed with 2% paraformaldehyde supplemented with 1.7% sucrose in phosphate buffer for 30 min at room temperature. After being permeabilized with 0.1% saponin in PBS, the cultures were incubated in serum-free medium supplemented with 1 mg/ml DNase I (Sigma) for 1 h at 37°C and then with 0.1 mg/ml of RNase A (Sigma) or vehicle for 1 h at 37°C. The cells were washed three times for 5 min each with TBS supplemented with 0.1% Triton X-100 and blocked with 10% (vol/vol) normal goat serum in PBS with 0.1% (vol/vol) saponin (blocking solution) for 1 h at room temperature and then incubated with primary antibody (mouse 15A3 at 1:200 in blocking solution; QED Bioscience, San Diego, CA) overnight at room temperature. After rinsing, the coverslips were incubated with secondary antibody solution (Alexa Fluor 488 goat anti-mouse IgG at 1:200 in blocking solution) for 90 min at room temperature. DNase I efficiency was controlled by nuclear staining with DAPI (4′,6-diamidino-2-phenylindole). The coverslips were then rinsed and mounted onto glass slides in Mowiol 4-88 supplemented with DABCO (1:5) as an antifade reagent and then visualized through a Leica TCS SP laser-scanning confocal microscope.

For immunoprecipitation experiments on 8-OHG containing rRNA, cells stably transfected with either APE1 shRNA- or scramble shRNA-encoding plasmids, were harvested after 10 days of doxycycline induction. Total RNA was isolated using Trizol reagent, according to the manufacturer's instructions. The RNA concentration was obtained spectrophotometrically, and RNA integrity was checked on agarose-formaldehyde gels. Oxidized RNA was immunoprecipitated as described before (46), with minor modifications. Briefly, 1.5 μg of total RNA was incubated with 2.5 μg of anti-8-OHG antibody 15A3 (QED Bioscience) in 200 μl of PBS supplemented with 400 U/ml RNaseOUT at room temperature for 1 h, and then 20 μl of protein G-Sepharose (Sigma) was added

and the samples were rocked for another 15 h at 4°C. The beads were spun down by centrifugation at 8,000 × *g* for 1 min at 4°C and washed three times by PBS with 0.04% (vol/vol) NP-40 (Sigma) (NP-40/PBS). The oxidized RNA/antibody/protein G complexes were resuspended into 200 μl of NP-40/PBS supplemented with 1% (wt/vol) SDS. RNA was isolated by adding 250 μl of Trizol reagent. The mixture was incubated for 15 min at 37°C with vortexing every 5 min, and then samples were further processed following the manufacturer's instructions. Immunoprecipitated RNAs and 1 μg of total input RNAs were reverse transcribed using the iScript cDNA synthesis kit (Bio-Rad) and then further analyzed by qRT-PCR as described before.

Northwestern analysis to evaluate the amount of 8-OHG was performed as previously reported (14), with modifications. As a control of the specificity of the detection analysis, a standard curve was also prepared with in vitro-oxidized RNA, as follows. Purified RNA (1.5 μg) was oxidized with increasing concentrations of H_2O_2 and cytochrome *c* (ratio of 16:1) for 1 h at 37°C as previously reported (45). RNA was denatured by addition of formamide (50%) and formaldehyde (2.2 M) and incubated for 15 min at 55°C. Samples were blotted onto Hybond-N^+ membrane (GE Healthcare) using a vacuum slot-blot apparatus (GE Healthcare) following the manufacturer's instructions. RNA was cross-linked to the membrane through UV irradiation (150 mJ). After blocking with 5% (wt/vol) nonfat dry milk in PBS–0.1% (wt/vol) Tween 20 for 1 h, the membrane was incubated with the anti-8-OHG primary antibody (QED Bioscience) for 1 h, followed by incubation with peroxidase-conjugated antimouse secondary antibody. The immunoreactive bands were detected using the ECL system.

AP site incision assays. The determination of AP endonuclease activity was performed using an oligonucleotide cleavage assay as described previously (64). Recombinant proteins were incubated with a 5′-^{32}P-end-labeled 26-mer oligonucleotide containing a single tetrahydrofuranyl (here called dsFDNA) artificial AP site at position 14, which is cleaved to a 14-mer in the presence of AP endonuclease activity. For the endonuclease assay with AP single-stranded RNA, we used the recently published (5) sequence 34FRNA (here designated as ssFRNA). Reactions from reaction mixtures (10 μl) containing the proteins of interest, 2.5 pmol of the 5′-^{32}P end-labeled oligonucleotide dsFDNA or ssFRNA, 50 mM HEPES, 50 mM KCl, 10 mM $MgCl_2$, 1 μg/μl bovine serum albumin, and 0.05% (wt/vol) Triton X-100 (pH 7.5) were allowed to proceed for 15 min in a 37°C water bath. Reactions were halted by adding 10 μl of 96% (vol/vol) formamide and 10 mM EDTA, with xylene cyanol and bromophenol blue as dyes. AP assay products (5 μl) were separated on a 20% polyacrylamide gel containing 7 M urea. Gels were wrapped in Saran wrap and exposed to film for autoradiography.

APE1 and NPM1 RNA binding assays. APE1 and NPM1 RNA complex formation was assessed as described previously (62), with assay mixtures incubated on ice for 10 min and separated on a native 8% (wt/vol) polyacrylamide gel at 120 V for 2 h. Each reaction mixture contained 2.5 pmol of RNA-labeled substrate and the indicated amount of proteins in a final volume of 10 μl.

Luciferase reporter assay. Luciferase mRNA was in vitro transcribed using T7 luciferase control DNA (Promega) as template and the T7 RiboMAX Express large-scale RNA production system (Promega), following the manufacturer's instructions. Cells expressing or not expressing endogenous APE1 were seeded on six-well plates 1 day before transfection and after 5 or 10 days of induction with doxycycline, at a cell density of 400,000 cells/well. Then, cells were transfected with 4 μg of in vitro-transcribed luciferase mRNA and 100 ng of β-galactosidase (β-Gal)-encoding vector for normalization of transfection efficiency (17) per well and using Lipofectamine 2000 reagent (Invitrogen), following the manufacturer's instructions. Cells were harvested 20 h after tranfection and lysed using 1× Promega cell culture lysis reagent. The luciferase assay was performed using the Promega luciferase assay system and a TD-20/20 luminometer (Turner BioSystems). Samples were normalized for total protein content by using Bio-Rad protein assay reagent and transfection efficiency was normalized by using a gene coding for cytomegalovirus (CMV)-β-Gal as a reporter gene.

rRNA labeling experiments. Equal numbers of APE1-knocked-down, WTAPE1- and NΔ33APE1-expressing HeLa cells (2×10^6) were labeled in medium containing 2.5 μCi/ml [^{3}H]uridine (Perkin-Elmer, Milan, Italy) for 30 min and then chased for the indicated times in label-free medium. Total RNA was isolated using Trizol reagent and loaded onto 1% (wt/vol) agarose-formaldehyde gels. RNA was transferred to Hybond N^+ membranes (GE Healthcare), cross-linked (150 mJ), sprayed with En^{3}Hance (Perkin-Elmer), and subjected to autoradiography.

Cell growth assay studies. For proliferation assays, cells were plated in triplicate, harvested at the indicated times upon doxycycline treatment, stained with trypan blue (Sigma), and counted. Colony survival assays were performed as previously described (41). Briefly, equal numbers (500 cells) of control and siRNA cells were plated in petri dishes and grown with medium containing or not containing doxycycline (1 μg/ml). On day 10, the medium was removed and colonies were stained for 2 min with 2 ml of crystal violet solution (10% [wt/vol] in 70% aqueous ethanol). The dye was then poured off. Then the plates were rinsed with tap water and allowed to dry. Colonies were counted by using ImageQuant TL software (GE Healthcare). For each experimental point, the mean, standard deviation, and statistical significance were calculated from three independent experiments.

Statistical analysis. Statistical analysis was performed using the Microsoft Excel data analysis program for Student's *t* test analysis. $P < 0.05$ was considered statistically significant.

RESULTS

Characterization of APE1 interactome map and role of the protein N-terminal sequence. To avoid stoichiometric problems due to overexpression of the bait protein and to increase the efficiency of the immunoprecipitation strategy, we developed a system in HeLa cells, in which the endogenous APE1 protein was substituted for by an ectopic Flag-tagged recombinant WT one. Silencing of the endogenous APE1 was performed by an inducible siRNA technology through a doxycycline-responsive promoter (58; and see Fig. S1 in the supplemental material). Ectopic expression was settled by stable cloning of an siRNA-resistant cDNA APE1 sequence. As the endogenous protein, ectopic WT APE1 localized mainly within the nuclear compartment of HeLa cell clones and was expressed to a similar extent (see Fig. S1C in the supplemental material), thus giving reliability to the approach used. To increase the resolution in the analysis of the immunoprecipitated complexes, a 2-DE separation of protein mixtures was performed. Figure 1A and Table 1 display the results of this analysis. As a control, we used immunoprecipitated material from HeLa cells stably transfected with the empty vector and expressing a scrambled siRNA sequence (see Materials and Methods for details and Fig. S2 in the supplemental material). Interestingly, among the 10 different protein species that were identified as being part of APE1 complexes (Fig. 1A), five of them (i.e., RLA0, NPM1, MEP50/WDR77, RSSA, and PRP19) are strictly related to RNA processing and ribosome biogenesis. Confirmatory data about interactions were obtained by coimmunofluorescence analysis (see Fig. S3 in the supplemental material). In particular, MEP50, K2C8, and PRDX6 were mainly localized at the cytoplasmic level in the majority of the cells; PRP19 was exclusively nuclear; and RLA0 displayed a pancellular distribution in both nuclear and cytoplasmic compartments.

With the aim of identifying the APE1-interacting partners modulated by the N-terminal 33 amino acid residues of the protein, a comparative coimmunoprecipitation analysis on NΔ33APE1- and WTAPE1-expressing cells was performed. We used the cell system described above, in which the endogenous APE1 protein was substituted for by an ectopic Flag-tagged recombinant protein, in both the WT and NΔ33 deletion mutant forms (see Fig. S1B in the supplemental material). Subcellular distribution of ectopic NΔ33APE1 resulted in both cytoplasmic and nuclear proteins, as a consequence of the lack of the bipartite NLS sequence (29) (see Fig. S1C in the supplemental material). Then, a differential proteomic strategy was used, by performing 2-DE separation of immunoprecipitated protein mixtures (Fig. 1B). In the NΔ33APE1 interactome map, particularly evident was the absence of nucleophosmin

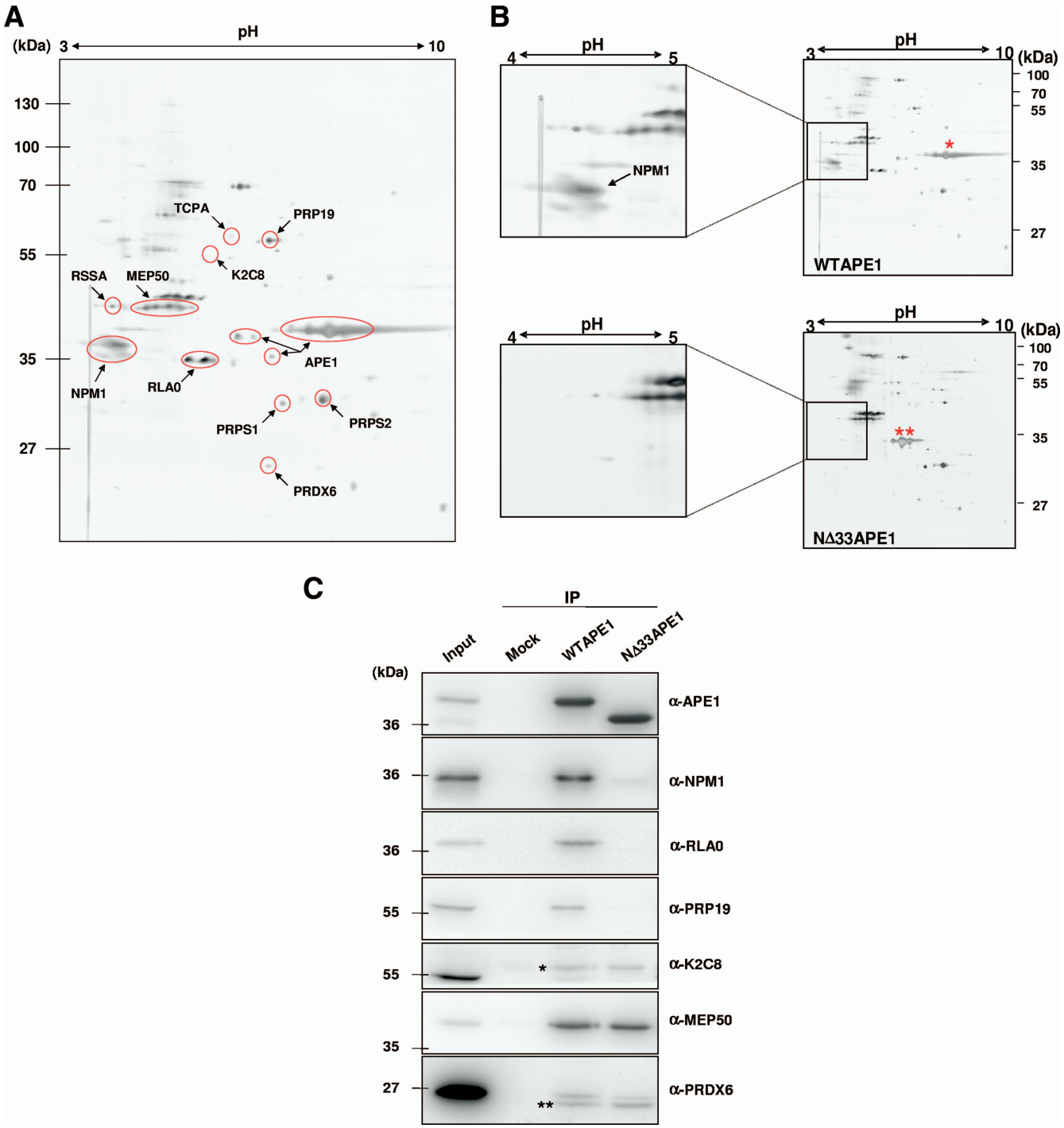

FIG. 1. NPM1 physically interacts with the 33 N-terminal amino acids of APE1. (A) 2-DE gel of the APE1-Flag protein complex immunopurified under native conditions from HeLa whole-cell lysate (20 mg from 4×10^7 cells). Results were obtained by silver staining and mass spectrometry identification of the proteins coimmunopurified with APE1-Flag. Highlighted are all of the proteins interacting specifically with APE1-Flag but not with the anti-Flag antibody. Names on the 2-DE map correspond to the proteins listed in Table 1. Vertical and horizontal axes indicate apparent molecular mass (kDa) and pI values, respectively. It has to be noticed that APE1-Flag protein is present in different focalized spots, as the consequence of different posttranslational modifications, including proteolysis of its N-terminal sequence. (B) 2-DE differential proteomic analysis of coimmunoprecipitated material identifies proteins interacting with the N-terminal sequence of APE1. Of particular interest was the identification of NPM1, whose interaction is lost upon removal of the first 33 N-terminal amino acids of APE1. An expanded view of silver-stained gel images of NPM1 shows the loss of interaction with the NΔ33APE1 protein. WT APE1-Flag and NΔ33APE1-Flag are indicated by one and two asterisks, respectively. (C) Western blotting analysis of the coimmunoprecipitated material. Total cell extracts from HeLa cells (Mock) and WT APE1 and NΔ33APE1 clones were coimmunoprecipitated. Coimmunoprecipitated material, after normalization for immunoprecipitated APE1 protein, was separated by 10% SDS-PAGE and analyzed by Western blotting to evaluate the levels of each interacting partner by using specific antibodies (shown as α-APE1, α-NPM1, etc.). In line 1, total cell extract was used as a positive control. Absence of signal in the "Mock" line confirmed the specificity of the interaction. Moreover, loss of NPM1 signal in the NΔ33 clone validates its interaction with the N-terminal region of APE1. Asterisks indicate the positions of Ig heavy (*) and light (**) chains used for the immunoprecipitation (IP) procedure, as demonstrated by separate Western blot analysis performed only with the secondary antibody (data not shown).

TABLE 1. APE1-interacting partners as detected by 2-DE and identified by peptide mass fingerprint analysis[a]

Protein identity (designation)[b]	Swiss Prot entry	Gene name	Experimental (theoretical) molecular mass in kDa	Experimental (hypothetical) pI	No. of spots	No. of peptides matched/ searched	Sequence coverage (%)	Estimated Z ProFound/Mascot score	Interaction with NΔ33APE1	Function
T-complex protein 1 subunit alpha (TCPA)	P17987	CCT1	57 (61)	5.4 (5.8)	1	10/13	20	2.23/138	No	Molecular chaperone
Pre-mRNA-processing factor 19 (PRP19)*	Q9UMS4	PRPF19	53 (55)	6.0 (6.1)	1	6/11	22	2.06/86	No	DNA double-strand break repair and pre-mRNA splicing reaction
Keratin, type II cytoskeletal 8 (K2C8)*	P05787	KRT8	50 (54)	5.1 (5.5)	1	9/11	12	2.23/116	No	Helps to link contractile apparatus to dystrophin at costameres of striated muscle
40S ribosomal protein SA (RSSA)	P08865	RPSA	38 (33)	4.5 (4.8)	1	7/13	22	2.10/103	↓	Belongs to ribosomal protein S2P family
Methylosome protein 50 (MEP50)*	Q9BQA1	WDR77	38 (37)	4.8 (5.0)	1	6/11	18	2.02/86	Yes	Component of 20S PRMT5-containing methyltransferase complex; might play role in transcription regulation
Nucleophosmin (NPM1)*	P06748	NPM1	35, 34, 34 (32.6)	4.6, 4.5, 4.7 (4.6)	3	9/13, 8/8, 7/7	19, 26, 14	2.29/100, 2.19/128, 1.86/103	No	Associated with nucleolar ribonucleoprotein structures and binding to single-stranded nucleic acids; assembly and transport of ribosome
DNA-apurinic/ apyrimidinic site lyase (APE1)*	P27695	APEX1	37, 34, 31 (35)	7.4, 5.5, 6.0 (8.4)	3	9/10, 7/10, 12/16	27, 30, 18	2.23/132;.05/96; 2.33/163	Not applicable	Repairs oxidative DNA damage in vitro
60S acidic ribosomal protein P0 (RLA0)*	P05388	RPLP0	34, 34, 34 (34)	5.0, 5.1, 5.2 (5.7)	3	7/7, 9/10, 10/14	13, 32, 40	1.94/122, 2.32/142, 2.38/157	No	Functional equivalent of *E. coli* protein L10
Ribose-phosphate pyrophosphokinase 1 (PRPS1)	P60891	PRPS1	31 (35)	7.0 (6.6)	1	8/8	29	2.28/115	Yes	Ribose metabolism
Ribose-phosphate pyrophosphokinase 2 (PRPS2)	P60891	PRPS2	31 (35)	6.4 (6.2)	1	6/7	19	1.93/103	Yes	Ribose metabolism
Peroxiredoxin 6 (PRDX6)*	P30041	PRDX6	25 (25)	6.0 (6.0)	1	7/8	37	2.18/131	↓	Involved in redox regulation of cell and protection against oxidative injury (lipid peroxidation)

[a] The protein name, accession number (SwissProt entry), gene name, experimental molecular mass and pI values (with corresponding theoretical values in parentheses), number of APE1 spots, number of peptides, sequence coverage, estimated Z ProFound and Mascot score, and known protein functions are listed. The protein's ability to interact with the NΔ33APE1 protein is also indicated. The down arrows indicate a decreased interaction with respect to WT APE1.

[b] An asterisk indicates the protein has been validated by Western blot analysis (Fig. 1C).

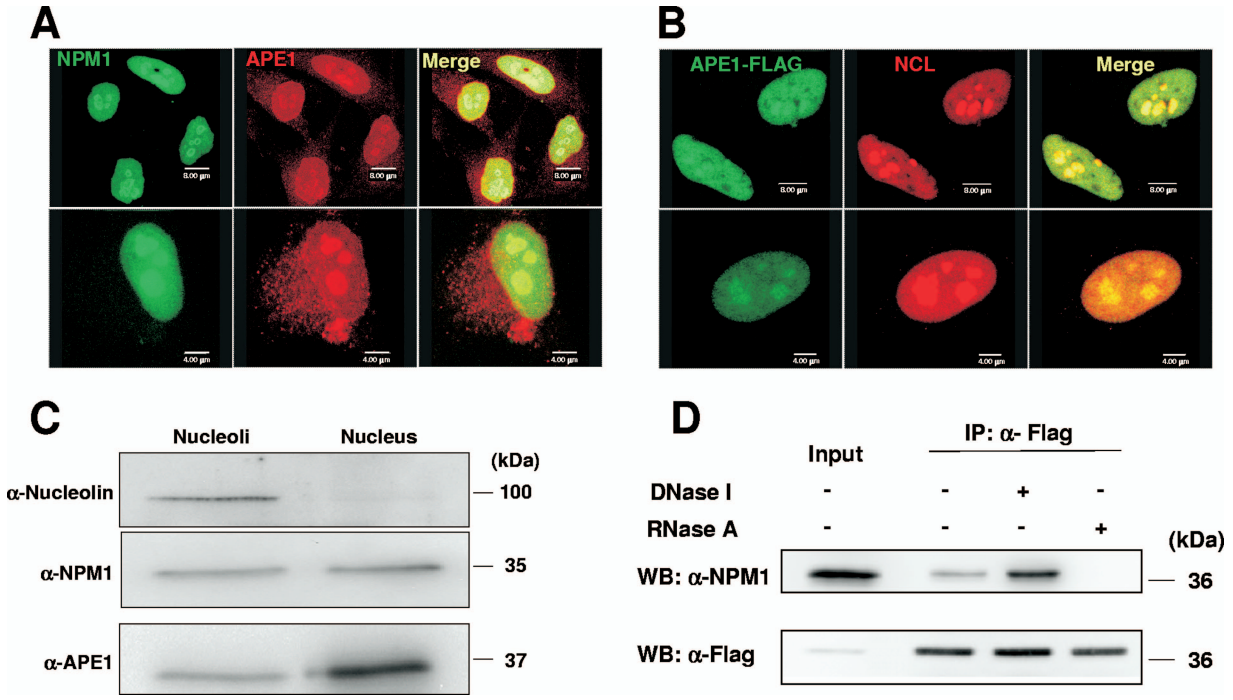

FIG. 2. APE1 is localized within nucleoli of HeLa cells and colocalizes and physically interacts with NPM1 and NCL in the granular region of the nucleolus. (A) Endogenous APE1 colocalizes with NPM1 in the granular region of the nucleolus. Confocal microscopy of WT HeLa cells fixed and stained with antibodies against NPM1 (green) and APE1 (red). Overlap of staining (yellow) demonstrated the colocalization of the two proteins. (B) HeLa cells transfected with the Flag-tagged APE1 cDNA-encoding plasmid were fixed and immunostained for NCL (red) and for APE1 (green). Merged images (yellow) show the localization of APE1 within nucleoli and colocalization with NCL. The Flag-tagged APE1 protein was detected with an anti-Flag antibody. (C) The biochemical isolation of nucleoli (37) confirms APE1 localization within these nuclear substructures (see Materials and Methods for details). Western blot (WB) analysis was performed on 10 μg of protein extracts, corresponding to 2×10^7 cell equivalents for the nucleolar fraction and to 2.5×10^5 cell equivalents for the nuclear fraction, respectively. α-Nucleolin, antinucleolin; α-NPM1, anti-NPM1; α-APE1, anti-APE1. (D) The interaction between APE1 and NPM1 is also mediated by RNA. HeLa cells were transfected with Flag-tagged APE1. Coimmunoprecipitation (IP) was performed using anti-Flag (α-Flag) monoclonal antibody-conjugated resin with identical aliquots of cell lysates. Cell lysates were pretreated with 100 U/ml DNase I and 100 μg/ml DNase-free RNase A for 30 min at 30°C before coimmunoprecipitation. Coimmunoprecipitates were separated onto a 12% SDS-PAGE gel and analyzed by Western blotting with the specific anti-NPM1 and anti-Flag antibodies.

(NPM1 or B23) (Fig. 1B, inset). Validation experiments with the identified protein species and evaluation of the effect of the N-terminus truncation on the other interacting partners identified so far (Fig. 1A) were performed by Western blot analysis on an independent set of immunoprecipitated material (Fig. 1C). Only in the case of MEP50 (Fig. 1C), PRPS1, and PRPS2 (Table 1) was the N-terminal sequence dispensable for the interaction with APE1.

APE1 is present within nucleoli and physically interacts with NPM1. Since NPM1 is a specific nucleolar protein (8), we inspected whether APE1 localizes within this subnuclear compartment. We performed colocalization analysis by immunofluorescence with NPM1 and with another nucleolar marker, nucleolin (NCL). HeLa cells were fixed, and nucleoli were visualized by confocal microscopy using antibodies against NCL or NPM1, which are localized mainly in the dense fibrillar regions and in the granular component of the nucleolus, respectively (8, 9, 48). Endogenous APE1 was visualized with a specific monoclonal antibody (39) in the case of colocalization with NPM1 (Fig. 2A) and with an anti-Flag antibody in the case of NCL (Fig. 2B). These experiments demonstrated that a significant portion of nuclear APE1 is concentrated within the nucleoli, colocalizing with both NCL and NPM1. The generalization of nucleolar localization of APE1 was confirmed by using several cell lines from different origins (see Fig. S4 in the supplemental material). A further biochemical validation was obtained by Western blot analysis of the proteins from purified HeLa cell nucleoli (38) (Fig. 2C).

Coimmunoprecipitation experiments performed on HeLa cells transfected with the Flag-tagged APE1 cDNA-encoding plasmid confirmed the physical interaction between APE1 and NPM1 and, to a lesser extent, that between APE1 and NCL (data not shown).

We then checked whether the APE1-NPM1 interaction involves RNA and/or DNA. For this purpose, cell lysates were digested with nuclease/RNase before coimmunoprecipitation. While DNase I treatment caused an increased interaction between the two proteins (possibly as a consequence of the change in the equilibrium involving APE1 binding to nucleic acids, which is moved from binding to DNA to binding to RNA upon treatment with DNase I), treatment with DNase-free chromatographically purified RNase A mostly reduced it (Fig. 2D; and see Fig. S5 in the supplemental material). The complex containing the two proteins was also dissociated by high salt concentration (data not shown). These data suggest that the strong interaction between APE1 and NPM1 may involve

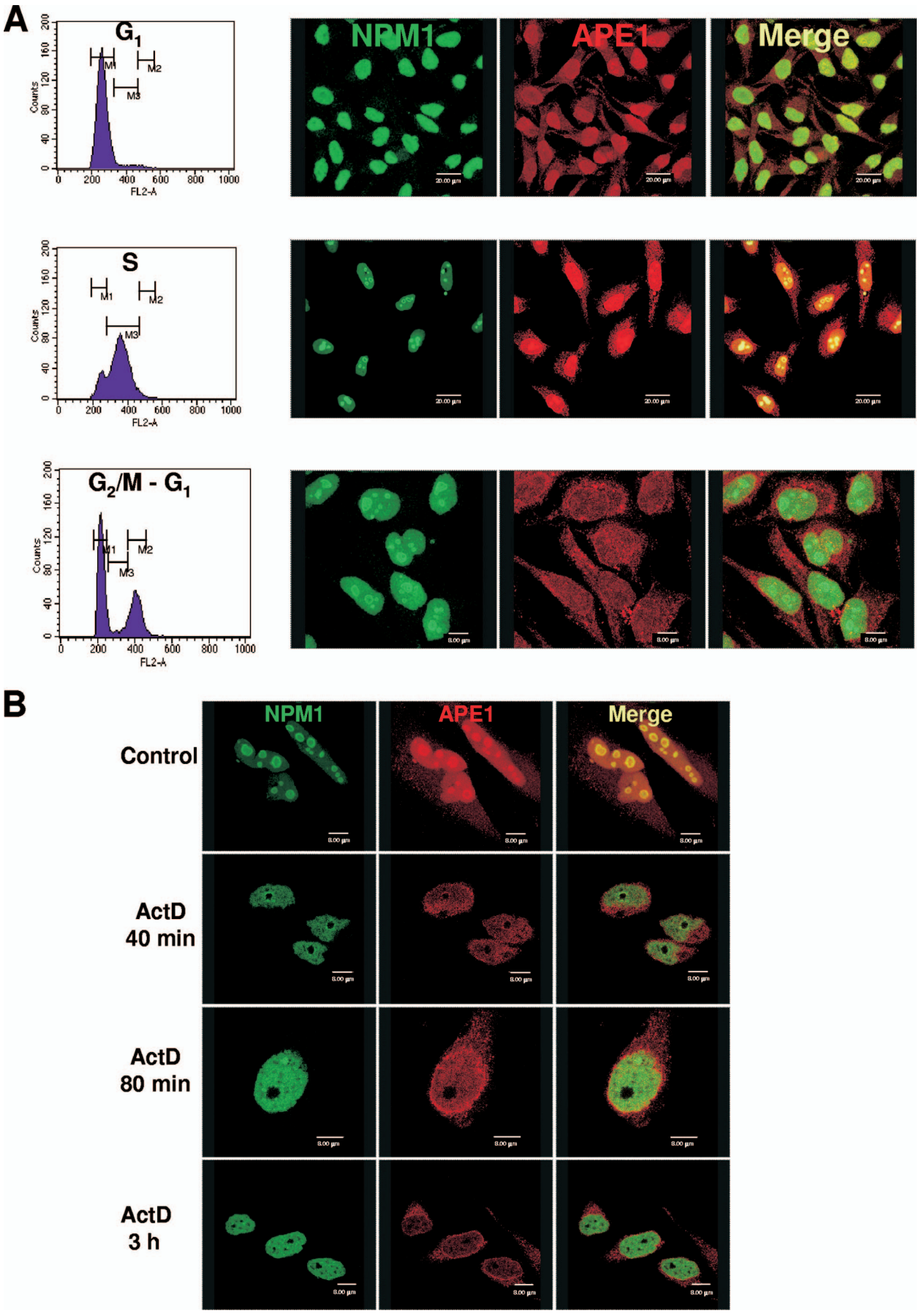

RNA molecules and is mediated by electrostatic interactions, as previously described for the interaction between NCL and NPM1 (40). Similar data on salt sensitivity and RNA dependence were also obtained for the two cytoplasmic proteins MEP50 and RLA0 (data not shown).

APE1 nucleolar localization is cell cycle dependent and requires active rRNA transcription. To determine if APE1-NPM1 interaction is associated with a particular biological process, we explored for their colocalization during the cell cycle. Cells were synchronized by the double-thymidine block, which arrests the cells at the G_1/S boundary. Cell samples were taken at different time points after release, and cell cycle progression was followed by flow cytometry. Samples were fixed and examined under a fluorescence microscope. Immediately after the removal of thymidine, most of the cells are at the G_1/S border. At this time, both APE1 and NPM1 are quite homogeneously distributed to the nucleus (Fig. 3A). As the cells progress through the S phase, 4 h after the double-thymidine block release, APE1 colocalizes with NPM1 within the nucleoli in most cells (Fig. 3A). Eleven hours upon release, cells overcome S phase and are distributed between G_2/M and the following G_1 phase. Cells in M phase do not show visible nucleoli according to the nuclear reorganization in mitosis. The cells shown in Fig. 3A (G_2/M-G_1) are likely to be in G_2 or G_1 phase, since they display a normal morphology. On the contrary, cells in M phase, which are rounded and weakly attached to the support, are not represented in this field. Eleven hours upon release from double-thymidine block, NPM1 is localized in the nucleoli, whereas APE1 shows a weak nuclear staining with no evident nucleolar localization. At this particular time point of release from the block, APE1 seems not to be preferentially localized in the nucleus, as in the G_1/S and S phases, but shows a diffuse staining with a punctate pattern in the perinuclear region. The biological significance of this peculiar APE1 localization at this specific point of cell cycle needs to be further investigated.

rRNA synthesis is mainly exerted during the S phase of the cell cycle. To evaluate if APE1 remains associated with the nucleolus in the absence of nascent rRNA transcription, we treated HeLa cells with ActD, which inhibits transcription by RNA polymerases I (Pol I), II, and III and causes disruption of the nucleolus (1), at a final concentration of 1 μg/ml and for different lengths of time. As expected, the disruption of the nucleolar structure was accompanied by the release of its components, as confirmed by the translocation of NPM1 to the nucleoplasm (Fig. 3B) and the translocation of APE1 in the perinuclear region. Inhibition of DNA synthesis with hydroxyurea did not elicit any effect on the nucleolar localization of APE1 (see Fig. S6A in the supplemental material), thus confirming that nucleolar localization of APE1 is specific for RNA metabolism. In addition, APE1 nucleolar localization strictly depends on RNA Pol I activity, as demonstrated by α-amanitin treatment at doses (10 μg/ml) inhibiting both RNA Pol II and III but not Pol I (see Fig. S6B in the supplemental material). Thus, APE1 nucleolar distribution accompanies rRNA synthesis during cell cycle progression.

The N-terminal homodimerization domain of NPM1 is responsible for APE1 interaction. We mapped the domain of NPM1 involved in the interaction with APE1 by GST-pull-down experiments. Several functional domains have been mapped in protein NPM1 (Fig. 4A), such as the homodimerization (Fig. 4A) and heterodimerization domains, and the nucleic acid binding domain (13). We tested the ability of five deletion mutants of NPM1 to bind APE1 in in vitro pull-down assays (Fig. 4B). We found that the first 117 N-terminal amino acid residues were essential for mediating NPM1-APE1 interaction. This region, spanning the homodimerization domain, is responsible for both oligomerization and chaperone activity of NPM1 (13, 49). Thus, the interaction between APE1 and NPM1 is largely dependent on the oligomerization domain of NPM1 and not on its nucleic acid binding region. To confirm our in vitro GST-pull-down assay experiments in an in vivo cell context, the two deletion mutants (positions 1 to 186 and 188 to 295) were expressed as Flag-tagged proteins in HeLa cells in transfection assays. The first mutant showed a nucleoplasmic/nucleolar localization just like the endogenous NPM1, while the latter was mislocated, showing mainly a nucleoplasmic localization, as previously reported (6). Coimmunofluorescence of endogenous APE1 and Flag-tagged NPM1 deletion mutants confirmed the GST-pull-down data (Fig. 4C). On the other hand, transfection of NΔ33APE1 showed no colocalization with NPM1 in the granular region of nucleoli (Fig. 4D), definitively demonstrating that the APE1 N terminus is involved in the APE1 subnuclear localization.

APE1 associates with 47S, 28S, and 18S rRNA. In order to evaluate the ability of APE1 and NPM1 to bind endogenous rRNA in the cell, we performed coimmunoprecipitation experiments separately for WT APE1, NΔ33APE1, and NPM1. The enrichment for the 47S, 28S, and 18S rRNA molecules, upon coimmunoprecipitation, was measured by qRT-PCR analysis (see Materials and Methods for details and Fig. 5A, left, for specific positioning of the PCR primers used for amplification). As shown in Fig. 5B to D, both WT APE1 and NPM1 were able to bind each of the rRNA molecules tested. Interestingly, the lower ability of the NΔ33APE1 deletion mutant to bind rRNA, although maintaining the nucleic acid binding domain at its C-terminal tail, suggested that the APE1 N terminus is required for APE1's ability to efficiently bind rRNA.

We tested the effect of RNA-binding ability of APE1 on HeLa cells by immunofluorescence analysis through RNase

FIG. 3. Interaction between APE1 and NPM1 is associated with cell cycle and requires active rRNA transcription. (A) Dynamic interaction of APE1 and NPM1 during the cell cycle in HeLa cells. HeLa cell cultures were synchronized by double-thymidine treatment. Samples were harvested either immediately (with most of the cells at the G_1/S border) or 4 h (most cells are in S phase) and 11 h after the removal of thymidine (with most cells distributed among G_2/M and the subsequent G_1 phases). (B) NPM1 and APE1 translocation induced by ActD. Shown are results obtained by confocal microscopy of WT HeLa cells fixed and stained with antibodies against NPM1 (green) and APE1 (red). Control cells show a bright nucleolar fluorescence, which indicates that NPM1 and APE1 are localized within nucleoli. After ActD treatment, the NPM1 nucleoplasmic fluorescence increased with time, indicating the NPM1 shifted from the nucleoli to the nucleoplasm. At the same time, the nucleolar staining of APE1 disappeared and the protein appeared to be concentrated in the perinuclear region.

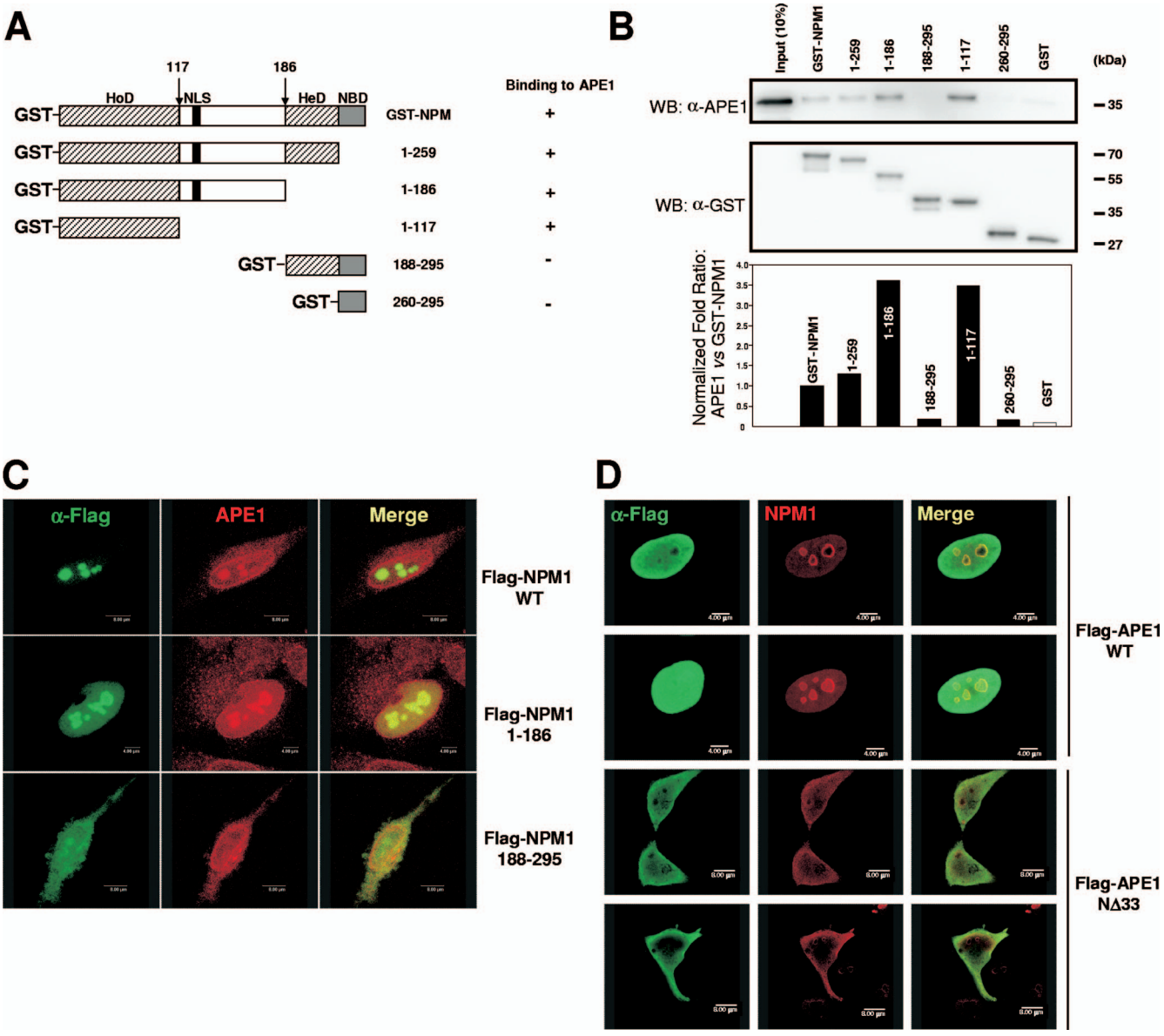

FIG. 4. Mapping of the APE1-interacting domain in NPM1. Interaction between APE1 and NPM1 requires the homodimerization domain of NPM1. (A) Domain structure of the full-length GST-NPM1 protein and the various deletion mutants used. HeD, heterodimerization domain; HoD, homodimerization domain; NBD, nucleic acid binding domain. (B) GST-pulldown assay on recombinant purified APE1 incubated with equivalent amounts of GST, GST-NPM1, or GST-derivatized deletion mutants. Results were analyzed by SDS-PAGE followed by Western blotting (WB) analysis with the specific anti-APE1 (α-APE1) antibody. α-GST, anti-GST. (C) Colocalization of NPM1 mutants with endogenous APE1 in HeLa cells. Cells were transfected with pcDNA5.1 expression vector containing Flag-tagged WT or mutant NPM1 variants. Ectopic proteins were detected by immunofluorescence with antibodies to the Flag epitope (green). APE1 was detected by the specific monoclonal antibody (red). (D) The NΔ33APE1 deletion mutant does not colocalize with NPM1 within nucleoli. HeLa cells were transfected with pcDNA5.1 expression vector containing the Flag-tagged WT or NΔ33APE1 deletion mutant. Shown are results obtained by confocal microscopy of WT HeLa cells fixed and stained with antibodies against NPM1 (red) and ectopic Flag-tagged APE1 (green). α-Flag, anti-Flag. Overlap of staining (yellow) demonstrates the colocalization of the two proteins.

treatment experiments after permeabilization (32). In control cells, besides in nucleoli, endogenous APE1 was mainly located within cellular nuclei (Fig. 5E, −RNase), in which it colocalized with a chromatin structure protein (i.e., the histone H3 isoform acetylated at Lys18, AcK18-H3). APE1 significantly relocalized to the cytoplasmic compartment upon RNase treatment (Fig. 5E, +RNase), although residual nuclear localization was observed. Treatment neither altered the nuclear and nucleolar structures nor affected DNA integrity, as proven by AcK18-H3 and NPM1 immunofluorescence (Fig. 5E, +RNase) and DAPI staining (see Fig. S5 in the supplemental material), thus demonstrating that this effect was due to RNA binding.

NPM1 stimulates APE1 endonuclease activity on abasic DNA but inhibits its endonuclease activity on RNA. NPM1 has chaperone activities on chromatin proteins (49); therefore, we

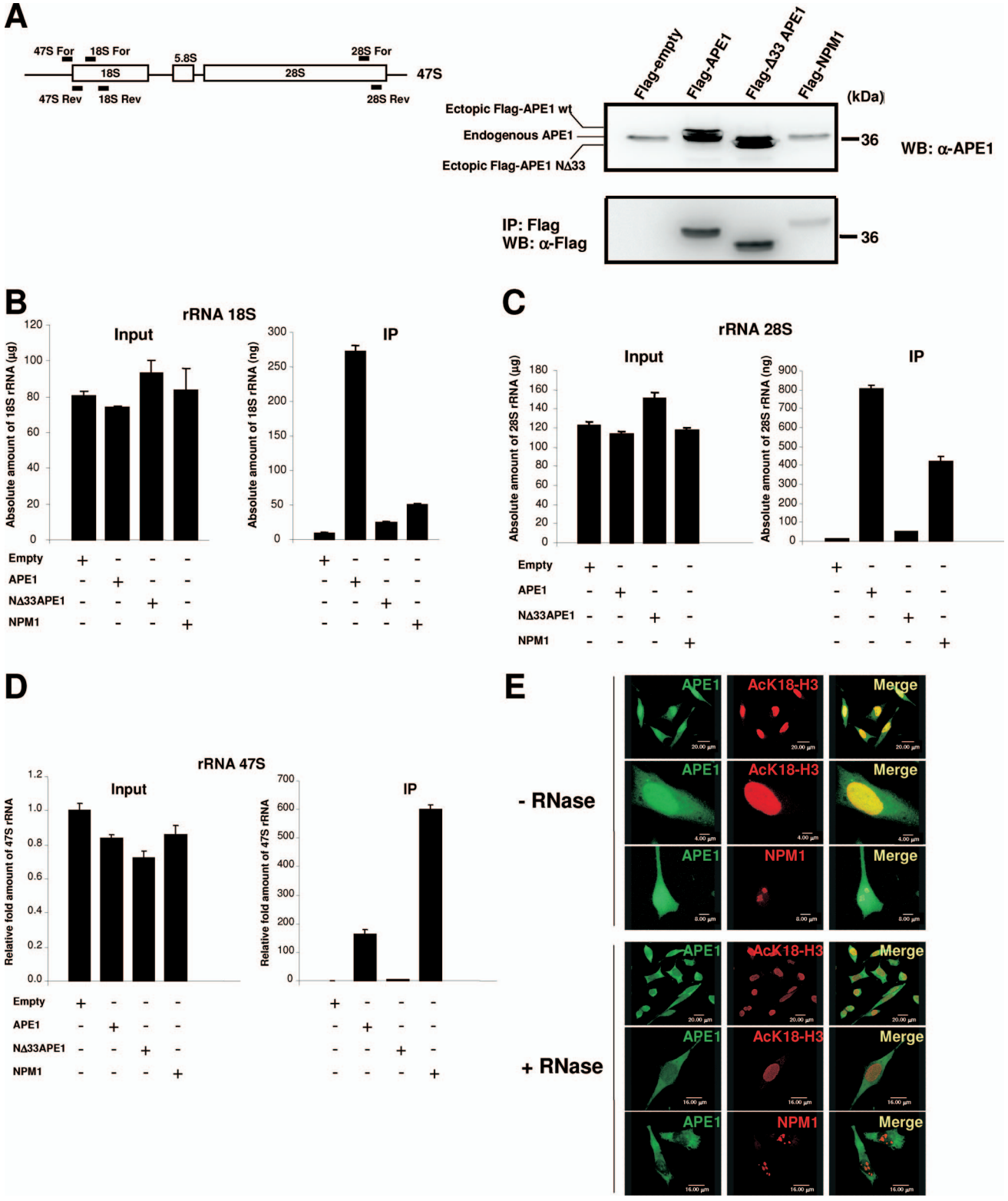

FIG. 5. APE1 associates with 47S, 28S, and 18S rRNA, and NPM1 competes with the binding. (A, left) Schematic representation of the 47S gene organization and position of the specific primers used for qRT-PCR analysis to quantitate the amount of each of the 47S, 28S, and 18S rRNA molecules present in the input and in the immunoprecipitated (IP) material of panels B to D. (Right) HeLa cells were transfected with WT APE1-Flag, NΔ33APE1-Flag, NPM1-Flag, or empty Flag vectors. Coimmunoprecipitation was performed, as described above, after normalization for the total amount of total RNA extracted. Aliquots of cell lysates and coimmunoprecipitates were used for Western (WB) blot analysis. α-Flag, anti-Flag. (B, C, and D) RNAs were extracted from immunoprecipitated material (as described for panel A, right), and the amounts of 47S, 28S, and 18S rRNA were evaluated by qRT-PCR analysis in the input and the immunoprecipitated fractions as well. (E) Nuclear localization of APE1 is dependent on the presence of an RNA component. After paraformaldehyde fixation, Triton X-100-permeabilized HeLa cells were treated with RNase A (+RNase) or mock treated (−RNase). Double-labeling immunofluorescence was carried out using anti-APE1 (α-APE1) and anti-AcK18-H3 or anti-NPM1 antibodies. The nuclei, as well as the nucleoli, are not screwed up by RNase treatment as the stainings of the nuclear component, acetylated H3 histone (AcK18-H3), and of the nucleolar component, NPM1, are preserved.

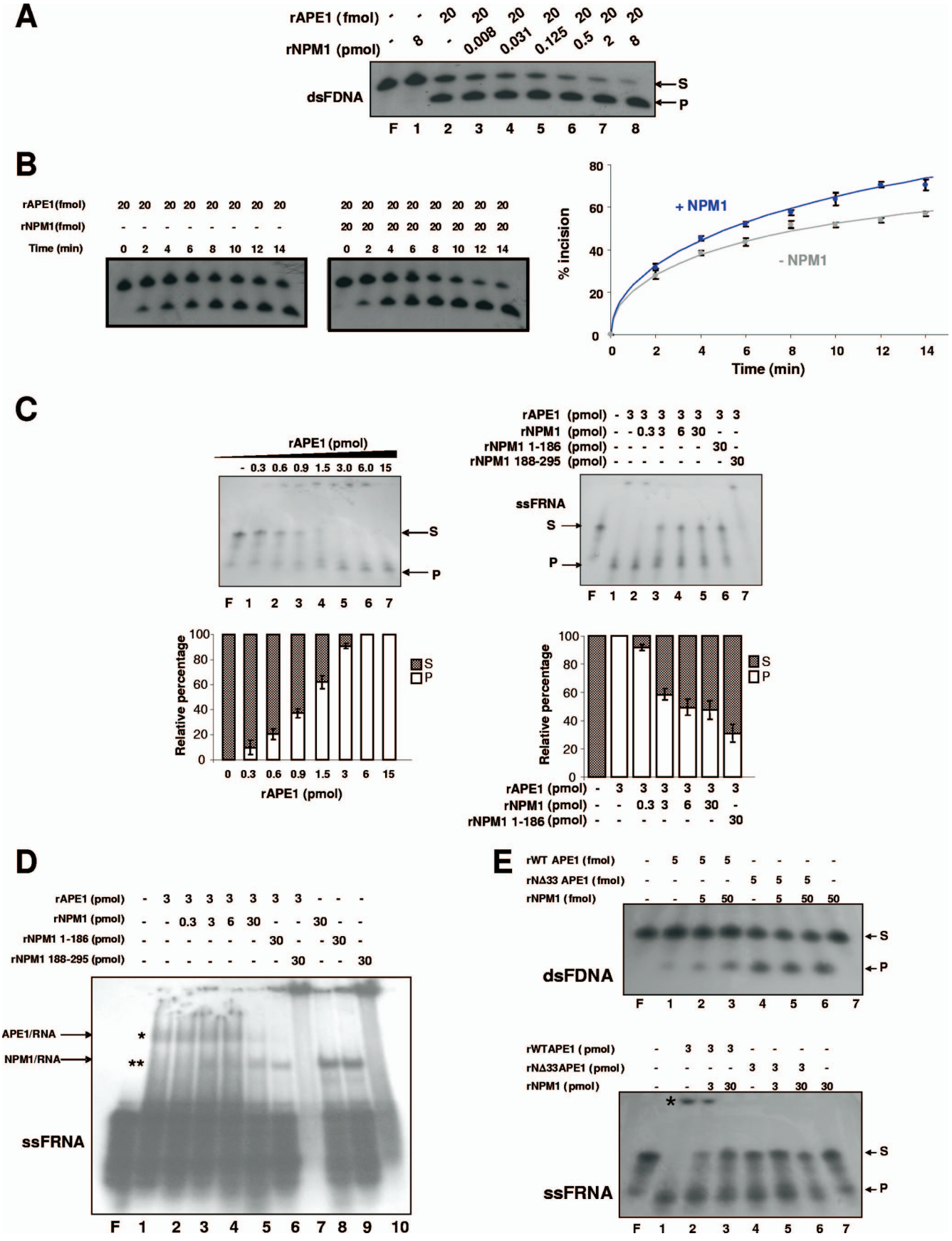

tested whether its interaction with APE1 may interfere with the endonuclease activity of the latter. The assay, as previously described (64), uses a radiolabeled double-stranded deoxyoligonucleotide (26-mer) containing an artificial tetrahydrofuran AP site which, when cleaved by AP endonuclease, produces a labeled 14-mer. The cleavage activity of a purified recombinant APE1 (rAPE1) was assayed in the presence/absence of purified recombinant NPM1 (rNPM1) protein. The results in Fig. 6A and B show the positive effects of NPM1 on the APE1 abasic DNA cleavage kinetics. A 10-fold excess of NPM1, which represents the physiological ratio as calculated from quantitative biochemical experiments (not shown), increased the APE1 endonuclease activity about threefold (see Fig. S7 in the supplemental material), thus reinforcing the physiologic importance of this interaction.

We then evaluated the effects of NPM1 on the cleavage by APE1 of an ssRNA containing a centrally located abasic site analogue. APE1 alone was able to incise a radiolabeled abasic single-stranded 34-mer RNA, ssFRNA (Fig. 6C, left), as recently demonstrated (5). Differently from what was seen for the abasic dsDNA, the purified recombinant NPM1 inhibited the rAPE1 endonuclease activity on abasic ssRNA in a concentration-dependent manner (Fig. 6C, right). The inhibition was obtained also in the presence of the two separated N-terminal (positions 1 to 186) and C-terminal (positions 188 to 295) domains of NPM1. Electrophoretic mobility shift assay (EMSA) analysis (Fig. 6D) demonstrated that the negative effect of NPM1 on the APE1 endonuclease activity on abasic RNA damage is due to an inhibitory effect of NPM1 over APE1 binding to ssFRNA. This effect was also evident in the presence of the N-terminal 1–186 interaction domain of NPM1, which, however, retained some ability to bind ssRNA (lane 9). Although experimental limitations prevent us from drawing any definitive conclusions, the inhibitory effect of the 188–295 NPM1 deletion mutant on the APE1 endonuclease activity on ssFRNA could be explained by the ability of this NPM1 mutant to form higher-order and very stable protein-RNA complexes, unable to enter the gel (lane 10). In the presence of full-length NPM1, since the decrease in APE1 binding to ssFRNA was not followed by a concomitant increase of NPM1/ssFRNA complex formation (Fig. 6D, lanes 2 to 5), we would argue that the inhibitory effect of NPM1 over APE1 RNA binding and RNA endonuclease activity may be explained on the basis of protein-protein interaction involving NPM1 and APE1, rather than a competitive squelching effect of NPM1 on RNA.

The role of APE1 interaction with NPM1 upon its ability to cleave dsFDNA and ssFRNA was evaluated by performing enzymatic assays with the NΔ33APE1 purified protein. Figure 6E shows that, as expected, the effect of NPM1 is completely lost with the NΔ33APE1 endonuclease activity on dsFDNA (upper) and ssFRNA (lower) (see Fig. S7 in the supplemental material). Interestingly, the 33 N-terminal residues of APE1 negatively modulate the APE1 endonuclease activity over dsFDNA, because NΔ33APE1 displays a higher (about 10-fold) enzymatic activity than the full-length protein (compare lanes 1 and 4 of Fig. 6E, upper panel; and see Fig. S7 in the supplemental material). In the case of ssFRNA, NΔ33APE1 shows lower enzymatic activity than the full-length protein (compare lanes 1 and 4 of Fig. 6E, lower panel). Thus, the APE1 N terminus is required for APE1 endonuclease activity on abasic RNA. The disappearance of the higher-order APE1/ssFRNA complexes, as obtained in the case of the NΔ33APE1 mutant, indicates a role for the N-terminal residues of the protein in the formation of a stable higher-order complex with ssFRNA. Overall, these data suggest that while in the case of dsDNA, NPM1 exerts a stimulatory effect on APE1 endonuclease activity over abasic sites, in the case of RNA, NPM1 plays a protective role and that, possibly, recognition of the abasic substrate, either DNA or RNA, may occur through different mechanisms. In the case of ssFRNA, this could imply a role of the nucleic acid's secondary structure (5).

In order to evaluate whether RNA quality may affect APE1's ability to bind it, we performed EMSA experiments with an intact RNA molecule (called ss34RNA) having the same sequence of the ssFRNA but devoid of the abasic site. The results in Fig. 7A show that while APE1 efficiently binds ss34RNA (with a dissociation constant of about 2×10^{-6} M), the NΔ33APE1 mutant does not. Assays using ss34RNA as

FIG. 6. APE1 endonuclease activity on abasic dsDNA and ssRNA is influenced by interaction with NPM1. (A) NPM1 interaction increases APE1 endonuclease activity on double-stranded AP DNA (dsFDNA). Reactions were performed as described in Materials and Methods with homogeneously purified recombinant proteins (rAPE1 and rNPM1) and stopped after 15 min of incubation at 37°C. The conversion of the radiolabeled tetrahydrofuran-containing oligonucleotide substrate (S) to the shorter incised product (P) was evaluated on a denaturing 20% (wt/vol) polyacrylamide gel. In each reaction, 2.5 pmol of dsFDNA was used. A representative image from three independent experiments is shown. F represents the free oligonucleotide probe without addition of enzyme. (B) Endonuclease kinetics of APE1 on dsFDNA is increased by interaction with NPM1. Reactions were performed as described for panel A, and proteins were incubated for the indicated times and separated on a denaturing 20% (wt/vol) polyacrylamide gel at 120 V for 2 h. In each reaction, 2.5 pmol of dsFDNA was used. Representative gels are reported on the left. Average values with standard deviations of three independent experiments are plotted on the right. (C, left) APE1 endonuclease activity on single-stranded abasic RNA (ssFRNA). Reactions were performed with purified recombinant proteins (rAPE1 and rNPM1) and stopped after 15 min of incubation at 37°C. In each reaction, 2.5 pmol of ssFRNA was used. The conversion of the radiolabeled abasic oligonucleotide substrate to the shorter incised product was evaluated on a denaturing 20% (wt/vol) polyacrylamide gel. A representative image from three independent experiments is shown. (Right) NPM1 (and its deletion mutants) inhibits APE1 endonuclease activity on single-stranded abasic ssFRNA. Reactions were performed and analyzed as described for the left panel. In each reaction, 2.5 pmol of ssFRNA was used. A representative image from three independent experiments is shown. (D) Binding of APE1 to ssFRNA is competed by NPM1. Reactions were performed with purified recombinant proteins (rAPE1 and rNPM1). The mixtures were separated on a native (nondenaturing) 8% (wt/vol) polyacrylamide gel at 120 V for 2 h. In each reaction, 2.5 pmol of ssFRNA was used. A representative EMSA gel image from three independent experiments, using the abasic ssFRNA sequence, is shown. An asterisk denotes the location of stable APE1-ssFRNA complexes. Two asterisks denote the location of stable NPM1-ssFRNA complexes. (E) Role of protein-protein interaction with NPM1 on the APE1 endonuclease activity on dsFDNA and ssFRNA. Enzymatic assays on dsFDNA (upper) and ssFRNA (lower) were performed as described for panels B and C. An asterisk on the lower image indicates the presence of higher-order stable complexes between WT APE1 and ssFRNA. A representative image from three independent experiments is shown.

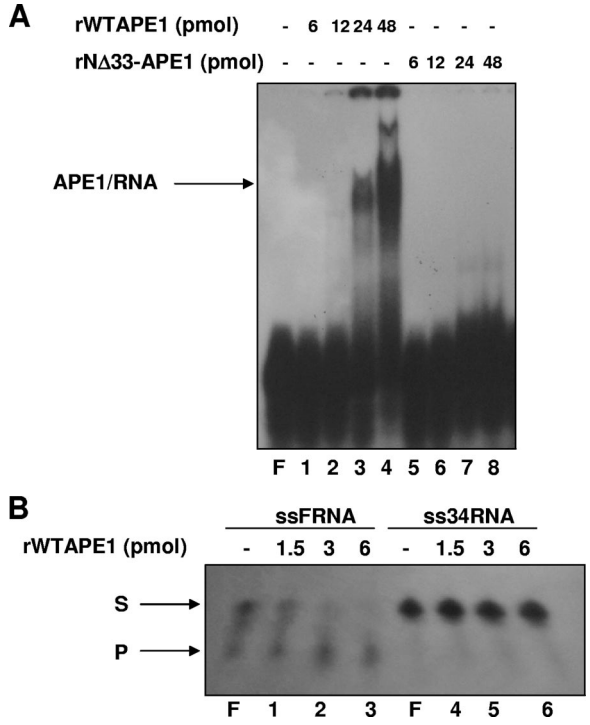

FIG. 7. APE1 efficiently binds but does not cleave the intact ss34RNA oligonucleotide. (A) Reactions were performed with purified recombinant proteins (rAPE1 and rNΔ33-APE1) and separated as described in the legend to Fig. 6D. ss34RNA is an intact oligonucleotide bearing the same sequence of ssFRNA but devoid of the abasic site. In each reaction, 2.5 pmol of intact ss34RNA was used. A representative EMSA gel image, from three independent experiments, is shown. F represents the free oligonucleotide probe without addition of enzyme. (B) APE1 does not cleave a single-stranded intact RNA (ss34RNA). Reactions were performed and separated as described for Fig. 6C. In each reaction, 2.5 pmol of ss34RNA or ssFRNA was used, as indicated.

substrate showed that, despite binding to this sequence, APE1 does not have an endonuclease activity on it (Fig. 7B). Thus, APE1 endonuclease activity on RNA requires the presence of an abasic site.

Overall, these data reinforce the role of the N terminus in mediating APE1 binding to RNA in addition to NPM1 and that the inhibitory effect of NPM1 over APE1 endonuclease over abasic RNA damage is exerted through mechanisms involving protein-protein interaction.

Loss of endogenous APE1 causes increased rRNA oxidation and reduces protein synthesis and cell proliferation. The biological relevance of our in vitro findings was evaluated by testing the ability to remove damaged (i.e., oxidized) RNA in cells not expressing APE1 upon oxidative treatment. HeLa cells were treated for 1 h with 50 or 200 μM H_2O_2 and then harvested 4 h after treatment. The amount of 8-OHG, the most abundant oxidized base (18), was evaluated by immunofluorescence analysis using a specific antibody (15A3) that recognizes 8-OHG modification in RNA, as previously reported (10, 46). In H_2O_2-treated cultures, the intensity of 15A3 immunofluorescence was significantly increased even at the lowest dose of H_2O_2 treatment, while being almost undetectable in untreated cells (Fig. 8A). Treatment with DNase I to remove possible immunoreactivity with 8-OHG on DNA, resulted in a very slight reduction of the signal (not shown). On the contrary, immunoreactivity was greatly reduced by RNase treatment, indicating RNA was the major site of nucleic acid oxidative damage.

Then, control, APE1-knocked-down, and WT APE1-reexpressing cells were treated for 1 h with 50 μM H_2O_2. After 4 h recovery, cells were harvested and RNA was extracted and purified. The amount of oxidized 18S rRNA molecules was evaluated by immunoprecipitation with the 15A3 antibody and quantified by qRT-PCR. Data reported in Fig. 8B (left), as well as those obtained with the 28S rRNA subunit (not shown), clearly show that accumulation of oxidized rRNA occurred as a consequence of APE1 silencing. Northwestern analysis, performed on the same samples of purified RNA, confirmed that higher levels of 8-OHG were associated with the loss of APE1 expression (Fig. 8B, right). Interestingly, the interaction between APE1 and NPM1 was reduced by H_2O_2 treatment, as demonstrated by coimmunoprecipitation assays (Fig. 8C), supporting the hypothesis that RNA damage modulates its and APE1's interaction with NPM1.

Mature and functional (nonoxidized) rRNA molecules are required for proper ribosome functioning in the protein synthesis processes (15, 26). In addition, mRNA oxidation causes inefficient elongation and/or premature termination of translation due to ribosome stalling (45, 53). Thus, we evaluated whether loss of endogenous APE1 may have any effect on the cellular protein translation processes. Comparison of the total protein content in cells lacking endogenous APE1 with that of control cells or cells reexpressing ectopic Flag-tagged WT APE1 (Fig. 8D, left) revealed that loss of APE1 caused a significant inhibition of protein translation processes. The results obtained by reporter assay experiments with in vitro-transcribed luciferase mRNA in APE1-deficient cells (Fig. 8D, right) strongly confirmed that the translation impairment following APE1 silencing is due to posttranscriptional mechanisms.

It is known that NPM1 is involved in ribosome biogenesis (27). Thus, considering (i) the interaction between APE1 and NPM1, (ii) the observed correlation between rRNA synthesis and APE1 localization, and (iii) the effect of APE1 silencing on protein synthesis, we asked whether the presence of APE1 or NΔ33APE1 could affect rRNA synthesis. Knocked-down HeLa cells, as well as WT APE1- and NΔ33APE1-expressing cells, were pulse-labeled with [^{3}H]uridine and chased for 30, 60, and 120 min to analyze the kinetics of newly synthesized rRNA. Then, their RNA was extracted and analyzed on gel (Fig. 8E). The pulse-labeled 47S rRNA precursor was readily detected in all samples at the beginning of chasing (0 min), indicating that transcription of the rRNA precursor was not blocked by APE1 downregulation. At the 60-min time point, the amount of mature 28S rRNA was approximately equal to the amount of 32S intermediate in all cell lines, with a 28S/32S ratio of approximately equal to 1. These data, showing that downregulation of APE1 or expression of the truncated protein did not alter the kinetics of rRNA processing but possibly led to formation of nonfunctional ribosomes, strongly suggest that APE1-NPM1 interaction may be part of a more general rRNA quality control process.

We then evaluated how the loss of APE1 functions in the

RNA-related process influences cell proliferation and viability. Cell counting and colony survival assays showed that NΔ33APE1-expressing cells displayed a significantly lower cell growth rate than WT APE1-expressing cells (Fig. 8F) and an intermediate growth rate compared with APE1-silenced cells. To define the impact of NΔ33APE1 expression on cell growth, we characterized cell cycle and apoptosis in reconstituted cells. Cell cycle characterization was performed through FACS analysis. Loss of APE1 impairs the passage from the S to G_2/M phases to the following G_1 phase, as measured by increase in S to G_2/M phases versus the G_1 population ratio (58). On the contrary, reconstituted cells did not show any significant difference between WT APE1- and NΔ33APE1-expressing cells (not shown). Cell death was characterized through apoptosis-specific assays (i.e., annexin V staining and caspase 3/7 activation). Both assays clearly demonstrated that cells expressing NΔ33APE1 show an increased apoptotic rate compared with WT APE1-expressing cells (Fig. 8G). Therefore, we can conclude that differences in cell growth between WT APE1- and NΔ33APE1-expressing cells are mainly due to increased death of the latter cells.

DISCUSSION

In this work, we have identified some of the APE1 interactome components under physiological cellular conditions, taking advantage of the cell system we developed in which endogenous APE1, silenced by the inducible expression of specific siRNA sequences, was replaced by a comparable amount of an ectopic siRNA-resistant Flag-tagged protein. Ten different proteins, among which was NPM1, mostly associated with RNA maturation and processing, were identified by proteomic analysis. We then focused our attention on the APE1/NPM1 complex and on the role played by this interaction in regulating APE1 endonuclease activity on abasic DNA or RNA and in the process of ribosome biogenesis and cell growth. We found an unsuspected role of APE1 in the rRNA quality control process that may open new perspectives in the comprehension of the nuclear and extranuclear functions of this protein, with a significant impact on human pathological processes such as neurodegenerative diseases and cancer.

Interestingly, we found that the first 33 N-terminal amino acids of APE1 are essential for stabilizing the interaction of APE1 with most of the identified partners, except MEP50, PRPS1, and PRPS2 (Table 1). While the C-terminal part of the protein is highly conserved during phylogeny, the N terminus is not (55, 56). Besides the mammalian proteins, in which the N terminus is highly conserved, this region is almost absent in other organisms, thus suggesting that it may represent a recent gain of function during evolution (55, 56). Based on our data and the awareness that this N-terminal sequence can be cleaved off under cellular stress conditions (11, 16, 23, 29, 66), we can infer that the unstructured amino-terminal sequence of APE1 is devoted to fine-tuning the different functions of APE1, mainly through modulation of its interactome network. The increased endonuclease activity, over abasic dsDNA, of NΔ33APE1 with respect to the full-length protein (Fig. 6E) and the observation that the APE1 N-terminal sequence is indispensable for its stable binding to RNA (Fig. 7A) further support the hypothesis that the N-terminal arm acts as a functional "switch" for modulating some of the different APE1 activities in mammalian cells.

A further important aspect resulting from this study is the subnuclear localization of APE1 within nucleoli as a consequence of the interaction with NPM1 and with the rRNA production process. Since rRNA synthesis and processing mostly occur at the G_1/S phase, compartmentalization of APE1 to the nucleoli during the S phase might increase the efficiency of ribosomal DNA (rDNA) transcription, through its BER activity, and/or the cleavage of abasic damaged rRNA molecules. In fact, APE1 is involved in the formation of a complex comprising NPM1 as well as precursor (47S) and mature (18S and 28S) rRNA molecules. Our EMSA experiments with purified recombinant APE1 protein suggest that APE1 may bind rRNA independently of NPM1 binding and that the N-terminal region is required for stable interaction with RNA molecules both in vivo (Fig. 5B to D) and in vitro (Fig. 7A).

Interaction with NPM1 in vitro stimulates APE1 endonuclease activity over abasic DNA, while it inhibits that on abasic RNA. What is the biological meaning of these results? Based on (i) the ability of NPM1 to stably bind to RNA but not to abasic dsDNA (not shown), (ii) the similar affinities of NPM1 and APE1 for abasic RNA (Fig. 6D, lane 3), and (iii) the presence of about 10-fold molar excess of NPM1 with respect to APE1 within nucleoli (not shown), it is conceivable that NPM1 may exert a fine-tuning control of APE1 endonuclease activity within nucleoli devoted to repair of AP damage on rDNA and the removal of oxidized rRNA molecules. Experiments are now in progress to demonstrate this possibility.

Based on our experimental data, we believe that the inhibitory effect of NPM1 over APE1 endonuclease activity on RNA may be explained on the basis of protein-protein interaction. In the absence of RNA damage, APE1 and NPM1 could be associated with RNA molecules. In the presence of an excess of NPM1 or a switching mechanism (such as a posttranslational modifications affecting APE1 N-terminus and/or NPM1) increasing the interaction between APE1 and NPM1, APE1 could be titrated away from RNA binding by NPM1, because the latter protein can mask the APE1 domain responsible for RNA binding. Alternatively, in the presence of an AP site formed on RNA, interaction between APE1 and NPM1 and/or NPM1 and RNA is weakened and APE1 may bind with increased affinity to the target RNA. The mode of NPM1 binding to RNA seems to be affected by RNA quality (abasic RNA is bound differently from undamaged RNA; data not shown); thus, NPM1 could be displaced from RNA binding. Therefore, competition of RNA and NPM1 for binding to APE1 N-terminal sequence may control the final outcome. Experiments are currently in progress to clarify this issue.

This picture does not hide the paramount role of APE1 on the RNA quality control process. The experimental data on support of this role are (i) the APE1 capacity of cleaving abasic RNA (5) (Fig. 6C, left), (ii) the accumulation of oxidized rRNA on APE1-defective cells (Fig. 8B), and (iii) the decreased APE1-NPM1 interaction in H_2O_2-damaged HeLa cells (Fig. 8C). Where and when the RNA cleansing process is carried out by APE1 depends on the relative local amounts of APE1 and NPM1 and on the extent of damage present in rRNA and rDNA within nucleoli. By this hypothesis, the

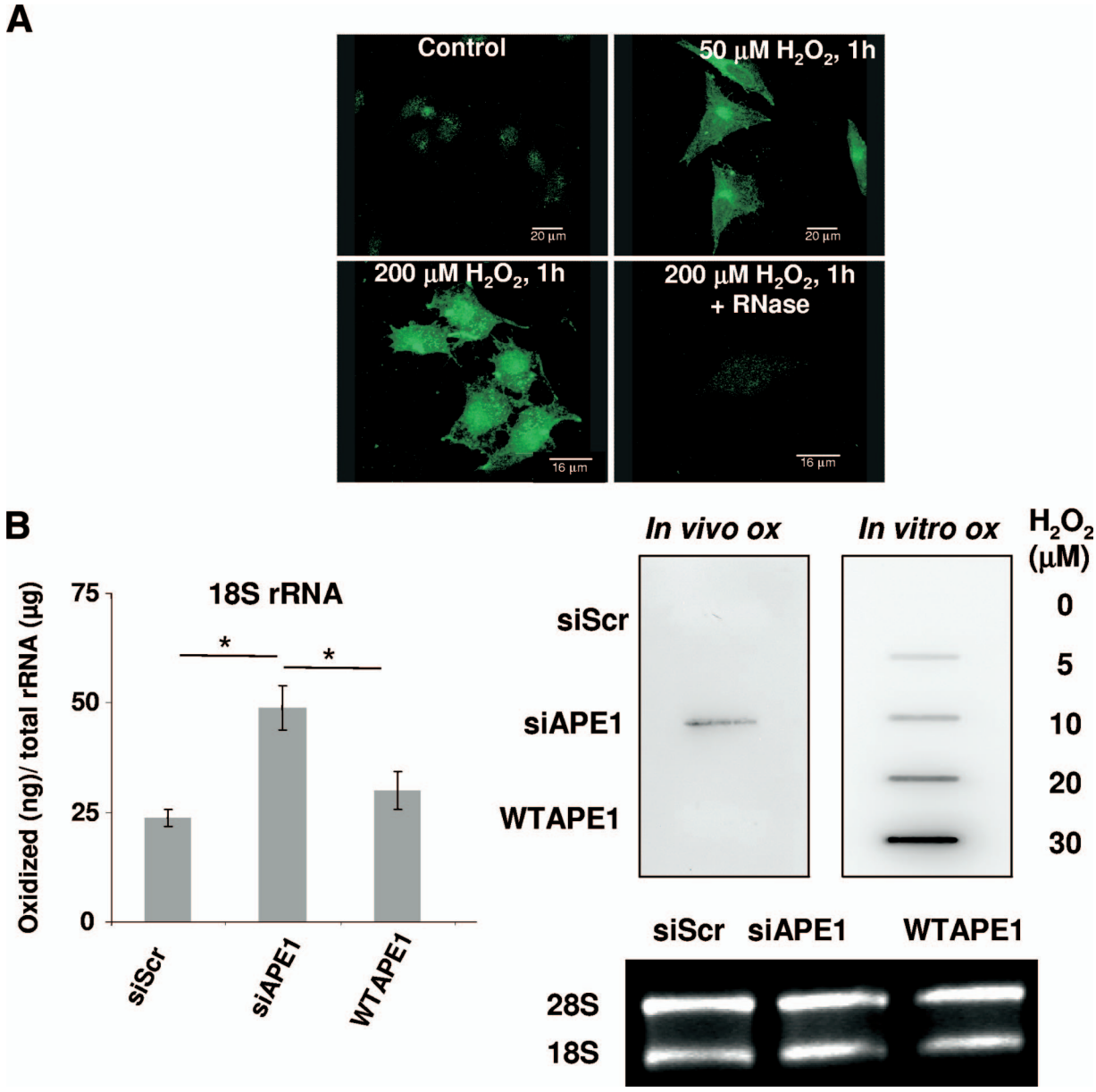

NPM1 affinity for damaged rRNA should diminish, whereas that of APE1 should increase with the extent of damage.

Why do APE1-defective cells have increased 8-OHG rRNA content upon oxidative stress? This can be explained only assuming that, besides spontaneous generation (31), enzymatic generation of abasic sites occurs upon rRNA oxidation. The existence of specific *N*-ribohydrolases, including the toxin ricin, has been already documented (44). A role for the YB-1 protein in recognizing 8-OHG sites has also been hypothesized (24), but no specific enzymatic mechanisms able to remove the oxidized base have been described yet. The accumulation of the 8-OHG substrates, which occurs upon silencing of APE1 expression, may thus be explained under the assumption that enzymatic removal of oxidized RNA bases represents the limiting step in the process. Interestingly, as hypothesized for DNA substrates, APE1 could be stimulating a glycosylase activity by allowing a faster turnover (61). Even though, due to the lack of a reliable method, we did not quantify the amount of abasic RNA damage, it is reasonable to postulate that in APE1-depleted cells the abasic RNA damage may also be increased as is abasic DNA damage (20, 58). Work is now undergoing to clarify these issues.

Due to its intrinsic nature (i.e., mostly single stranded and with bases not protected by hydrogen bonding or binding to specific proteins) and to its relative larger amount, RNA may be more susceptible to oxidative insults than DNA (36). Not only 8-OHG but also 5-hydroxycytidine, 5-hydroxyuridine, and 8-hydroxyadenosine have been identified in oxidized RNA (65). If not repaired, these kinds of damage causing altered pairing may lead to ribosomal dysfunctions and erroneous

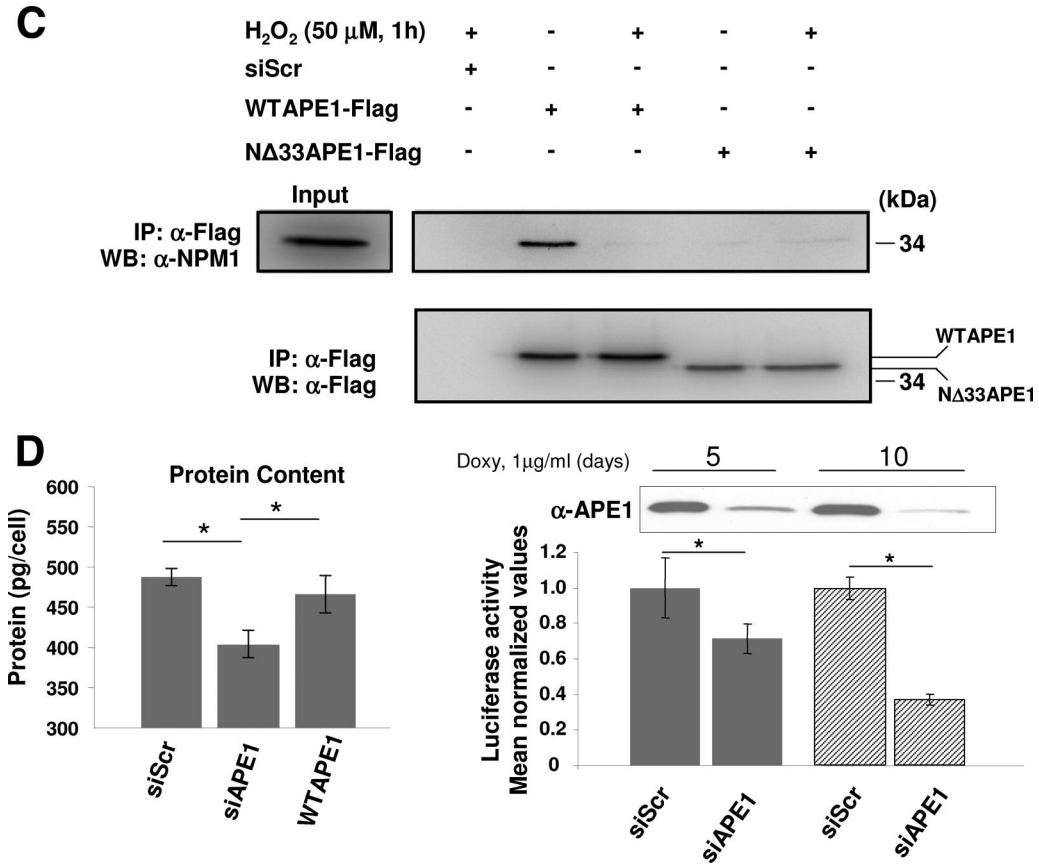

FIG. 8. Loss of endogenous APE1 causes increased rRNA oxidation and reduces protein synthesis and cell proliferation. (A) RNA oxidation occurs in H_2O_2-treated cells. HeLa cells were exposed to the indicated doses of H_2O_2 for 1 h, followed by a recovery period of 4 h. RNA oxidation was detected by 15A3 immunofluorescence staining. The immunoreactivity was greatly diminished by the RNase treatment. All samples were DNase I treated. (B) Accumulation of oxidatively damaged rRNA in APE1-knocked-down cells. (Left) Quantitative analysis of the amount of rRNA oxidation in 15A3-immunoprecipitated RNAs by qRT-PCR analysis. Control represents HeLa cells stably transfected with a scrambled shRNA sequence (siScr), siAPE1 represents HeLa cells stably transfected with a specific shRNA sequence to inhibit endogenous APE1 expression, WT APE1 represents cells expressing only the ectopic APE1 protein in spite of the endogenous one (see Materials and Methods) (58). Inducible silencing of endogenous APE1 was obtained through doxycycline (1 μg/ml) treatment for 10 days as described in Materials and Methods and reference 58. HeLa cells (2×10^6) were treated for 1 h with 50 μM H_2O_2 and released for 4 h. Analysis of 8-OHG-containing RNA is described in Materials and Methods. Levels of oxidation (ox) of 18 S rRNA are higher in APE1-silenced than in APE1-expressing cells, supporting the hypothesis that APE1 plays a role in cleansing of damaged RNA within mammalian cells. Data are means ± standard deviations from three independent experiments. *, $P < 0.05$. (Right) 15A3 antibody-based dot blot Northwestern detection of 8-OHG was used to analyze the amount of oxidized RNA in the total RNA pool from expressing and nonexpressing HeLa cells, treated as described above. As a loading control, the bands corresponding to 28S and 18S rRNA were visualized by ethidium bromide staining of the gel before transfer. In vitro oxidation of purified RNA with different amounts of H_2O_2 was used to demonstrate the specificity of the assay used. (C) RNA oxidation impairs APE1-NPM1 interaction. Coimmunoprecipitation (IP) experiments were performed on HeLa cells stably expressing WT APE1-Flag or NΔ33APE1-Flag proteins and treated as described for panel B. Then the presence of NPM1 protein in the immunoprecipitated material was evaluated by Western blotting (WB). α-Flag, anti-Flag; α-NMP1, anti-NMP1. (D, left) After 10 days of doxycycline treatment, HeLa cells (5×10^5) were harvested and analyzed for protein content by a standard colorimetric Bradford assay. HeLa cell clones were as described for panel 8B. (Right) Control (siScr) or nonexpressing (siAPE1) endogenous APE1 HeLa cells were transfected with in vitro-transcribed luciferase mRNA. Normalized luciferase activity as a function of the total protein levels is reported. Experimental details are described in Materials and Methods. The endogenous level of APE1 protein was evaluated by Western blot analysis on the total cell extract. α-APE1, anti-APE1. Data, expressed as the change (fold) with respect to control cultures, are means ± standard deviations from three independent experiments. *, $P < 0.05$. (E) Silencing (siAPE1) or expression of truncated APE1 (NΔ33APE1) does not affect rRNA synthesis as determined by pulse-chase experiments. HeLa cells as control cells (siScr), nonexpressing cells (siAPE1), or cells expressing only the WT or APE1 deletion mutant (NΔ33APE1) were obtained as described in Materials and Methods and reference 58 and treated with doxycycline (1 μg/ml) for 10 days. Then the cells were pulse-labeled with [^{3}H]uridine for 30 min and chased for the indicated times. An equal amount of RNA was loaded into each lane. The ratios of densitometric signals of 28S to 32S, calculated by a PhosphorImager, are shown. (F) Effect of APE1 silencing on cell proliferation and role of the N-terminal 33-amino-acid sequence. HeLa cell clones were as described for panel E. Cells were treated for different times with doxycycline (1 μg/ml), and then cell growth was measured. (Left) Growth was monitored through direct cell counting by measuring the cell number at various times after doxycycline (Doxy) treatment. Data are means ± standard deviations from three independent experiments. *, $P < 0.05$. (Right) Cell growth as measured by colony survival assay. Five hundred cells of the control and siRNA clones were seeded in petri dishes and then treated with doxycycline for 10 days. Data, expressed as the percentage of change with respect to control cultures, are means ± standard deviations from three independent experiments. *, $P < 0.05$. (G) Loss of the 33 N-terminal amino acids within APE1 sequence affects cell death. HeLa cell clones were as described for panel E. Apoptosis was measured through caspase 3/7 activation (left) and annexin V (right) assays. The histograms show the average ± standard deviation of the fluorescence values (relative fluorescence units [RFU]) obtained from three independent experiments. *, $P < 0.05$.

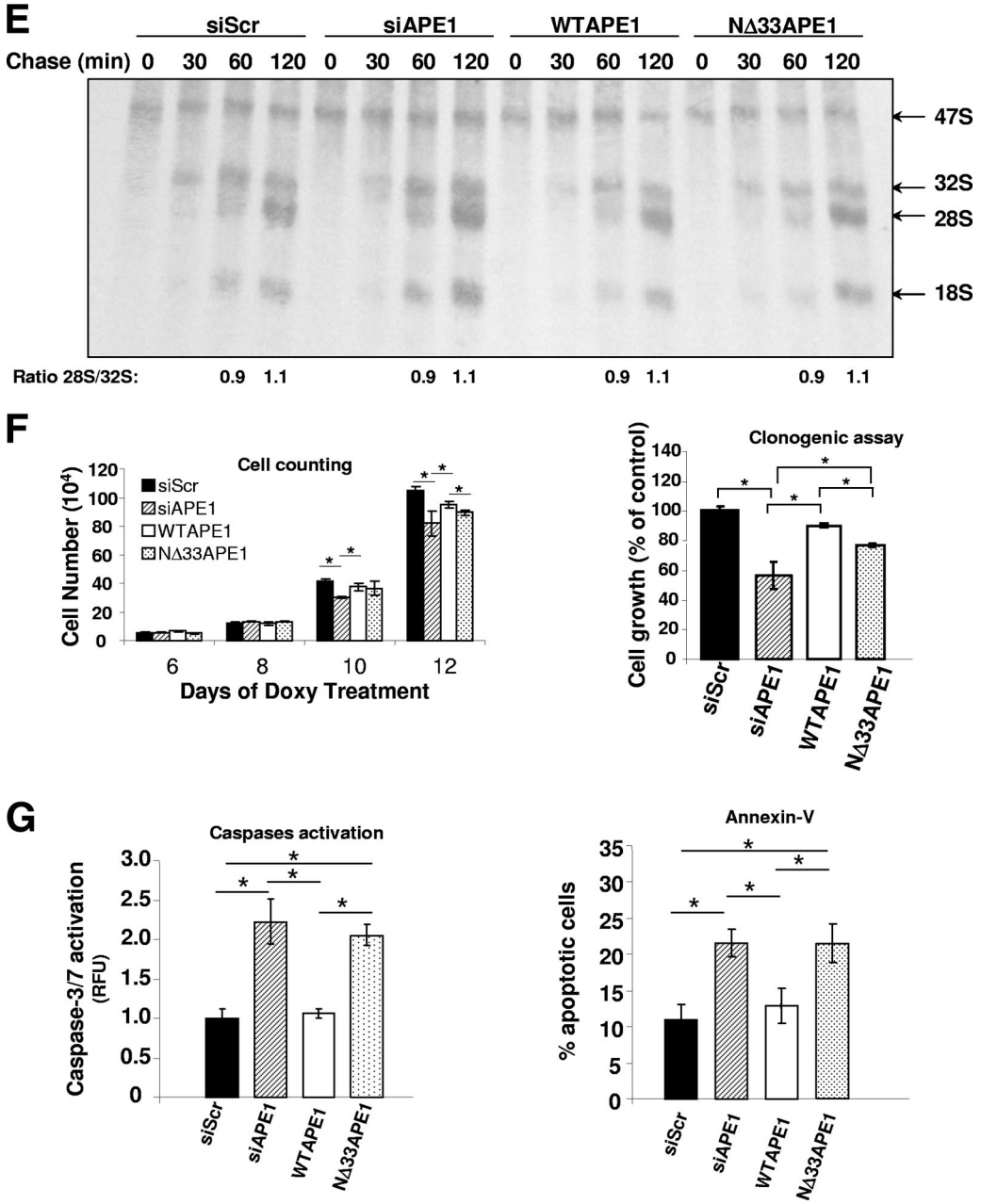

FIG. 8—*Continued.*

translation process, thus significantly affecting the overall protein synthesis mechanism (15, 53). In agreement with this hypothesis, we found a significant reduction in the protein synthesis rate upon silencing of APE1 expression (Fig. 8D). RNA damage, in turn, causes cell cycle arrest and cell death, with or without the contribution of p53 and inhibition of protein synthesis (4). From our data, the RNA-binding function of APE1, which is specifically controlled through interaction by means of its N-terminal sequence, seems to have a significant impact on cell viability (Fig. 8F and G).

The new and striking findings of APE1 interaction with RNA and with proteins involved in ribosome assembly (i.e., RLA0 and RSSA) and RNA maturation (i.e., PRP19 and MEP50) within cytoplasm could also represent a molecular explanation for the "extranuclear" functions of this protein. Its RNA-mediated association with these proteins would reinforce the hypothesis of APE1 as an essential factor in the RNA quality control process. Future studies will elucidate whether this hypothesis could also explain the cytoplasmic accumulation of APE1 in a number of tumor cell types (55, 56).

Oxidative damage to RNA molecules, both coding for proteins (mRNA) or performing translation (rRNA and tRNA), has recently been associated with the occurrence of neurodegenerative diseases such as Alzheimer's disease (36) and its impact in cancer development could not be excluded, at present (4). Thus, all of the hypotheses made about the in-

volvement of APE1 in the development of such pathologies should be reinterpreted in light of our findings. The role that APE1 has in RNA-related processes needs further study, but due to its ability to recognize and cleave through its endonuclease activity the RNA AP sites (see our present data and reference 5), its role is compatible with a leading role in the early stages of the RNA quality control process. Little information is still available on the molecular mechanisms responsible for specific recognition and removal of damaged RNA (4), in particular abasic RNA. Our data clearly point to APE1 as a novel enzyme responsible for the "cleansing" process to degrade and remove the abasic RNA molecules, which may play a leading role in the control of RNome functionality, in association with hAlkB and YB-1.

ACKNOWLEDGMENTS

This work was supported by grants from MIUR (FIRB RBRN 07BMCT and the Italian Human Proteome Network) and Telethon (GGP06268) to G.T. and CNR (AG.P04.015, MERIT, and RSTL 862) to A.S.

We greatly thank Sankar Mitra for fundamental support in the development of this work.

REFERENCES

1. **Andersen, J. S., Y. W. Lam, A. K. L. Leung, S. E. Ong, C. E. Lyon, A. I. Lamond, and M. Mann.** 2005. Nucleolar proteome dynamics. Nature **433:** 77–83.
2. **Apicelli, A. J., L. B. Maggi, Jr., A. C. Hirbe, A. P. Miceli, M. E. Olanich, C. L. Schulte-Winkeler, A. J. Saporita, M. Kuchenreuther, J. Sanchez, K. Weilbaecher, and J. D. Weber.** 2008. A non-tumor suppressor role for basal $p19^{ARF}$ in maintaining nucleolar structure and function. Mol. Cell. Biol. **28:**1068–1080.
3. **Beernink, P. T., B. W. Segelke, M. Z. Hadi, J. P. Erzberger, D. M. Wilson III, and B. Rupp.** 2001. Two divalent metal ions in the active site of a new crystal form of human apurinic/apyrimidinic endonuclease, Ape1: implications for the catalytic mechanism. J. Mol. Biol. **307:**1023–1034.
4. **Bellacosa, A., and E. G. Moss.** 2003. RNA repair: damage control. Curr. Biol. **13:**R482–R484.
5. **Berquist, B. R., D. R. McNeill, and D. M. Wilson III.** 2008. Characterization of abasic endonuclease activity of human Ape1 on alternative substrates, as well as effects of ATP and sequence context on AP site incision. J. Mol. Biol. **379:**17–27.
6. **Bertwistle, D., M. Sugimoto, and C. J. Sherr.** 2004. Physical and functional interactions of the Arf tumor suppressor protein with nucleophosmin/B23. Mol. Cell. Biol. **24:**985–996.
7. **Bhakat, K. K., T. Izumi, S. H. Yang, T. K. Hazra, and S. Mitra.** 2003. Role of acetylated human AP-endonuclease (APE1/Ref-1) in regulation of the parathyroid hormone gene. EMBO J. **1:**6299–6309.
8. **Biggiogera, M., S. Fakan, S. H. Kaufmann, A. Black, J. H. Shaper, and H. Busch.** 1989. Simultaneous immunoelectron microscopic visualization of protein B23 and C23 distribution in the HeLa cell nucleolus. J. Histochem. Cytochem. **37:**1371–1374.
9. **Chan, P. K., W. Y. Chan, B. Y. Yung, R. G. Cook, M. B. Aldrich, D. Ku, I. L. Goldknopf, and H. Busch.** 1986. Amino acid sequence of a specific antigenic peptide of protein B23. J. Biol. Chem. **261:**14335–14341.
10. **Chang, Y., Q. Kong, X. Shan, G. Tian, H. Ilieva, D. W. Cleveland, J. D. Rothstein, D. R. Borchelt, P. C. Wong, and C. L. Lin.** 2008. Messenger RNA oxidation occurs early in disease pathogenesis and promotes motor neuron degeneration in ALS. PLoS ONE. **3:**e2849.
11. **Chattopadhyay, R., L. Wiederhold, B. Szczesny, I. Boldogh, T. K. Hazra, T. Izumi, and S. Mitra.** 2006. Identification and characterization of mitochondrial abasic (AP)-endonuclease in mammalian cells. Nucleic Acids Res. **34:**2067–2076.
12. **Chung, U., T. Igarashi, T. Nishishita, H. Iwanari, A. Iwamatsu, A. Suwa, T. Mimori, K. Hata, S. Ebisu, E. Ogata, T. Fujita, and T. Okazaki.** 1996. The interaction between Ku antigen and REF1 protein mediates negative gene regulation by extracellular calcium. J. Biol. Chem. **271:**8593–8598.
13. **Colombo, E., J. C. Marine, D. Danovi, B. Falini, and P. G. Pelicci.** 2002. Nucleophosmin regulates the stability and transcriptional activity of p53. Nat. Cell Biol. **4:**529–533.
14. **Ding, Q., E. Dimayuga, W. R. Markesbery, and J. N. Keller.** 2004. Proteasome inhibition increases DNA and RNA oxidation in astrocyte and neuron cultures. J. Neurochem. **91:**1211–1218.
15. **Ding, Q., W. R. Markesbery, Q. Chen, F. Li, and J. N. Keller.** 2005. Ribosome dysfunction is an early event in Alzheimer's disease. J. Neurosci. **25:**9171–9175.
16. **Fan, Z., P. J. Beresford, D. Zhang, Z. Xu, C. D. Novina, A. Yoshida, Y. Pommier, and J. Lieberman.** 2003. Cleaving the oxidative repair protein Ape1 enhances cell death mediated by granzyme A. Nat. Immunol. **4:**145–153.
17. **Fantini, D., C. Vascotto, M. Deganuto, N. Bivi, S. Gustincich, G. Marcon, F. Quadrifoglio, G. Damante, K. K. Bhakat, S. Mitra, and G. Tell.** 2008. APE1/Ref-1 regulates PTEN expression mediated by Egr-1. Free Radic. Res. **42:**20–29.
18. **Fiala, E. S., C. C. Conaway, and J. E. Mathis.** 1989. Oxidative DNA and RNA damage in the livers of Sprague-Dawley rats treated with the hepatocarcinogen 2-nitropropane. Cancer Res. **49:**5518–5522.
19. **Frehlick, L. J., J. M. Eirin-Lòpez, and J. Ausiò.** 2007. New insights into the nucleophosmin/nucleoplasmin family of nuclear chaperones. Bioessays **29:** 49–59.
20. **Fung, H., and B. Demple.** 2005. A vital role for Ape1/Ref1 protein in repairing spontaneous DNA damage in human cells. Mol. Cell **17:**463–470.
21. **Gorman, M. A., S. Morera, D. G. Rothwell, E. de La Fortelle, C. D. Mol, J. A. Tainer, I. D. Hickson, and P. S. Freemont.** 1997. The crystal structure of the human DNA repair endonuclease HAP1 suggests the recognition of extrahelical deoxyribose at DNA abasic sites. EMBO J. **16:**6548–6558.
22. **Grillo, C., C. D'Ambrosio, A. Scaloni, M. Maceroni, S. Merluzzi, C. Turano, and F. Altieri.** 2006. Cooperative activity of Ref-1/APE and ERp57 in reductive activation of transcription factors. Free Radic. Biol. Med. **41:**1113–1123.
23. **Guo, Y., J. Chen, T. Zhao, and Z. Fan.** 2008. Granzyme K degrades the redox/DNA repair enzyme Ape1 to trigger oxidative stress of target cells leading to cytotoxicity. Mol. Immunol. **45:**2225–2235.
24. **Hayakawa, H., T. Uchiumi, T. Fukuda, M. Ashizuka, K. Kohno, M. Kuwano, and M. Sekiguchi.** 2002. Binding capacity of human YB-1 protein for RNA containing 8-oxoguanine. Biochemistry **41:**12739–12744.
25. **He, T., N. L. Weintraub, P. C. Goswami, P. Chatterjee, D. M. Flaherty, F. E. Domann, and L. W. Oberley.** 2003. Redox factor-1 contributes to the regulation of progression from G0/G1 to S by PDGF in vascular smooth muscle cells. Am. J. Physiol. Heart Circ. Physiol. **285:**804–812.
26. **Honda, K., M. A. Smith, X. Zhu, D. Baus, W. C. Merrick, A. M. Tartakoff, T. Hattier, P. L. Harris, S. L. Siedlak, H. Fujioka, Q. Liu, P. I. Moreira, F. P. Miller, A. Nunomura, S. Shimohama, and G. Perry.** 2005. Ribosomal RNA in Alzheimer disease is oxidized by bound redox-active iron. J. Biol. Chem. **280:**20978–20986.
27. **Itahana, K., K. P. Bhat, A. Jin, Y. Itahana, D. Hawke, R. Kobayashi, and Y. Zhang.** 2003. Tumor suppressor ARF degrades B23, a nucleolar protein involved in ribosome biogenesis and cell proliferation. Mol. Cell **12:**1151–1164.
28. **Izumi, T., D. B. Brown, C. V. Naidu, K. K. Bhakat, M. A. Macinnes, H. Saito, D. J. Chen, and S. Mitra.** 2005. Two essential but distinct functions of the mammalian abasic endonuclease. Proc. Natl. Acad. Sci. USA **102:**5739–5743.
29. **Jackson, E. B., C. A. Theriot, R. Chattopadhyay, S. Mitra, and T. Izumi.** 2005. Analysis of nuclear transport signals in the human apurinic/apyrimidinic endonuclease (APE1/Ref1). Nucleic Acids Res. **33:**3303–3312.
30. **Kuninger, D. T., T. Izumi, J. Papaconstantinou, and S. Mitra.** 2002. Human AP-endonuclease 1 and hnRNP-L interact with a nCaRE-like repressor element in the AP-endonuclease 1 promoter. Nucleic Acids Res. **30:**823–829.
31. **Loeb, L. A., and B. D. Preston.** 1986. Mutagenesis by apurinic/apyrimidinic sites. Annu. Rev. Genet. **20:**201–230.
32. **Maison, C., D. Bailly, A. Peters, J. P. Q. Quivy, D. Roche, A. Taddei, M. Lachner, T. Jenuwein, and G. Almouzni.** 2002. Higher-order structure in pericentric heterochromatin involves a distinct pattern of histone modification and an RNA component. Nat. Genet. **30:**329–334.
33. **Mitra, S., T. Izumi, I. Boldogh, K. K. Bhakat, R. Chattopadhyay, and B. Szczesny.** 2007. Intracellular trafficking and regulation of mammalian AP-endonuclease 1 (APE1), an essential DNA repair protein. DNA Repair (Amsterdam) **6:**461–469.
34. **Mittal, V.** 2004. Improving the efficiency of RNA interference in mammals. Nat. Rev. Genet. **5:**355–365.
35. **Mol, C. D., T. Izumi, S. Mitra, and J. A. Tainer.** 2000. DNA-bound structures and mutants reveal abasic DNA binding by APE1 and DNA repair coordination. Nature **403:**451–456.
36. **Moreira, P. I., A. Nunomura, M. Nakamura, A. Takeda, J. C. Shenk, G. Aliev, M. A. Smith, and G. Perry.** 2008. Nucleic acid oxidation in Alzheimer disease. Free Radic. Biol. Med. **44:**1493–1505.
37. **Muramatsu, M., K. Smetana, and H. Busch.** 1963. Quantitative aspects of isolation of nucleoli of the Walker carcinosarcoma and liver of the rat. Cancer Res. **25:**693–697.
38. **Parlanti, E., G. Locatelli, G. Maga, and E. Dogliotti.** 2007. Human base excision repair complex is physically associated to DNA replication and cell cycle regulatory proteins. Nucleic Acids Res. **35:**1569–1577.
39. **Pines, A., L. Perrone, N. Bivi, M. Romanello, G. Damante, M. Gulisano, M. R. Kelley, F. Quadrifoglio, and G. Tell.** 2005. Activation of APE1/Ref-1 is dependent on reactive oxygen species generated after purinergic receptor stimulation by ATP. Nucleic Acids Res. **33:**4379–4394.

40. **Piñol-Roma, S.** 1999. Association of nonribosomal nucleolar proteins in ribonucleoprotein complexes during interphase and mitosis. Mol. Biol. Cell **10:**77–90.
41. **Plumb, J. A.** 1999. Cell sensitivity assays: clonogenic assay. Cytotoxic drug resistance mechanisms. Humana Press, Totowa, NJ.
42. **Reardon, B. J., C. R. Lombardo, and M. Sander.** 1998. Drosophila Rrp1 domain structure as defined by limited proteolysis and biophysical analyses. J. Biol. Chem. **273:**33991–33999.
43. **Savkur, R. S., and M. O. Olson.** 1998. Preferential cleavage in pre-ribosomal RNA byprotein B23 endoribonuclease. Nucleic Acids Res. **26:**4508–4515.
44. **Schramm, V. L.** 1997. Enzymatic N-riboside scission in RNA and RNA precursors. Curr. Opin. Chem. Biol. **1:**323–331.
45. **Shan, X., H. Tashiro, and C. L. Lin.** 2003. The identification and characterization of oxidized RNAs in Alzheimer's disease. J. Neurosci. **23:**4913–4921.
46. **Shan, X., Y. Chang, and C. L. Lin.** 2007. Messenger RNA oxidation is an early event preceding cell death and causes reduced protein expression. FASEB J. **21:**2753–2764.
47. **Shevchenko, A., M. Wilm, O. Vorm, and M. Mann.** 1996. Mass spectrometric sequencing of proteins silver-stained polyacrylamide gels. Anal. Chem. **68:** 850–858.
48. **Srivastava, M., P. J. Fleming, H. B. Pollard, and A. L. Burns.** 1989. Cloning and sequencing of the human nucleolin cDNA. FEBS Lett. **250:**99–105.
49. **Swaminathan, V., A. H. Kishore, K. K. Febitha, and T. K. Kundu.** 2005. Human histone chaperone nucleophosmin enhances acetylation-dependent chromatin transcription. Mol. Cell. Biol. **25:**7534–7545.
50. **Szczesny, B., and S. Mitra.** 2005. Effect of aging on intracellular distribution of abasic (AP) endonuclease 1 in the mouse liver. Mech. Ageing Dev. **126:**1071–1078.
51. **Szebeni, A., K. Hingorani, S. Negi, and M. O. Olson.** 2003. Role of protein kinase CK2 phosphorylation in the molecular chaperone activity of nucleolar protein b23. J. Biol. Chem. **278:**9107–9115.
52. **Takeuchi, R., T. Ruike, R. Nakamura, K. Shimanouchi, Y. Kanai, Y. Abe, A. Ihara, and K. Sakaguchi.** 2006. Drosophila DNA polymerase zeta interacts with recombination repair protein 1, the Drosophila homologue of human abasic endonuclease 1. J. Biol. Chem. **281:**11577–11585.
53. **Tanaka, M., P. B. Chock, and E. R. Stadtman.** 2007. Oxidized messenger RNA induces translation errors. Proc. Natl. Acad. Sci. USA **104:**66–71.
54. **Tell, G., E. Crivellato, A. Pines, I. Paron, C. Pucillo, G. Mancini, A. Bandiera, M. R. Kelley, C. Di Loreto, and G. Damante.** 2001. Mitochondrial localization of APE/Ref-1 in thyroid cells. Mutat. Res. **485:**143–152.
55. **Tell, G., F. Quadrifoglio, C. Tiribelli, and M. R. Kelley.** 2009. The many functions of APE1/Ref-1: not only a DNA-repair enzyme. Antioxid. Redox Signal. [Epub ahead of print.] doi:10.1089/ars.2008.2194.
56. **Tell, G., G. Damante, D. Caldwell, and M. R. Kelley.** 2005. The intracellular localization of APE1/Ref-1: more than a passive phenomenon? Antioxid. Redox Signal. **7:**367–384.
57. **van de Wetering, M., I. Oving, V. Muncan, M. T. Pon Fong, H. Brantjes, D. van Leenen, F. C. Holstege, T. R. Brummelkamp, R. Agami, and H. Clevers.** 2003. Specific inhibition of gene expression using a stably integrated, inducible small-interfering-RNA vector. EMBO Rep. **4:**609–615.
58. **Vascotto, C., L. Cesaratto, L. A. H. Zeef, M. Deganuto, C. D'Ambrosio, A. Scaloni, M. Romanello, G. Damante, G. Taglialatela, D. Delneri, M. R. Kelley, S. Mitra, F. Quadrifoglio, and G. Tell.** 29 January 2009. Genome-wide analysis and proteomic studies reveal APE1/Ref-1 multifunctional role in mammalian cells. Proteomics [Epub ahead of print.] doi:10.1002/pmic.200800638.
59. **Vascotto, C., L. Cesaratto, C. D'Ambrosio, A. Scaloni, C. Avellini, I. Paron, U. Baccarani, G. L. Adani, C. Tiribelli, F. Quadrifoglio, and G. Tell.** 2006. Proteomic analysis of liver tissues subjected to early ischemia/reperfusion injury during human orthotopic liver transplantation. Proteomics **6:**3455–3465.
60. **Vidal, A. E., S. Boiteux, I. D. Hickson, and J. P. Radicella.** 2001. XRCC1 coordinates the initial and late stages of DNA abasic site repair through protein-protein interactions. EMBO J. **20:**6530–6539.
61. **Vidal, A. E., I. D. Hickson, S. Boiteux, and J. P. Radicella.** 2001. Mechanism of stimulation of the DNA glycosylase activity of hOGG1 by the major human AP endonuclease: bypass of the AP lyase activity step. Nucleic Acids Res. **29:**1285–1292.
62. **Wilson, D. M., III.** 2003. Properties of and substrate determinants for the exonuclease activity of human apurinic endonuclease Ape1. J. Mol. Biol. **330:**1027–1037.
63. **Xanthoudakis, S., G. G. Miao, and T. Curran.** 1994. The redox and DNA-repair activities of Ref-1 are encoded by nonoverlapping domains. Proc. Natl. Acad. Sci. USA **91:**23–27.
64. **Yacoub, A., M. R. Kelley, and W. A. Deutsch.** 1997. The DNA repair activity of human redox/repair protein APE/Ref-1 is inactivated by phosphorylation. Cancer Res. **57:**5457–5459.
65. **Yanagawa, H., Y. Ogawa, and M. Ueno.** 1992. Redox ribonucleosides. Isolation and characterization of 5-hydroxyuridine, 8-hydroxyguanosine, and 8-hydroxyadenosine from Torula yeast RNA. J. Biol. Chem. **267:**13320–13326.
66. **Yoshida, A., Y. Urasaki, M. Waltham, A. C. Bergman, P. Pourquier, D. G. Rothwell, M. Inuzuka, J. N. Weinstein, T. Ueda, E. Appella, I. D. Hickson, and Y. Pommier.** 2003. Human apurinic/apyrimidinic endonuclease (Ape1) and its N-terminal truncated form (AN34) are involved in DNA fragmentation during apoptosis. J. Biol. Chem. **278:**37768–37776.
67. **Ziel, K. A., V. Grishko, C. C. Campbell, J. F. Breit, G. L. Wilson, and M. N. Gillespie.** 2005. Oxidants in signal transduction: impact on DNA integrity and gene expression. FASEB J. **19:**387–394.